OUTLINE OF THE INCOHERENT SCATTER METHOD

Tuomo Nygrén

Department of Physics, University of Oulu

Finland

EISCAT Summer School
Sodankylä, Finland
August 30 – September 3, 2010

Fourier presentation of a signal

A signal $x(t)$ can be presented in terms of its Fourier transform

$$X(\nu) = \mathcal{F}\{x(t)\} = \int_{-\infty}^{\infty} x(t)e^{-i\omega t}\, dt \tag{1}$$

in the form

$$x(t) = \mathcal{F}^{-1}\{X(\nu)\} = \int_{-\infty}^{\infty} X(\nu)e^{i\omega t}\, d\nu. \tag{2}$$

Here ν is the frequency and $\omega = 2\pi\nu$ the angular frequency. We say that $x(t)$ and $X(\nu)$ make a Fourier transform pair. When $x(t)$ is real,

$$X^*(\nu) = \int_{-\infty}^{\infty} x(t)e^{i\omega t}\, dt = X(-\nu). \tag{3}$$

In terms of the modulus $|X(\nu)|$ and phase angle $\varphi(\nu)$ this can be written as

$$|X(\nu)|e^{-i\varphi(\nu)} = |X(-\nu)|e^{i\varphi(-\nu)} \tag{4}$$

or

$$\begin{aligned} |X(-\nu)| &= |X(\nu)| \\ \varphi(-\nu) &= -\varphi(\nu). \end{aligned} \tag{5}$$

These relations are not valid for a complex signal $z(t)$.

Filtering a signal

A filter is a linear system which is completely described by its impulse response. The impulse response is defined as the output signal corresponding to an input signal equal to the Dirac delta function.

Assume $x(t)$ is the input signal in a linear system with an impulse response $h(t)$. The task is to calculate the output signal $y(t)$. Using the definition of the delta function, we can write

$$x(t) = \int_{-\infty}^{\infty} x(\tau)\delta(\tau - t)d\tau = \int_{-\infty}^{\infty} x(\tau)\delta(t - \tau)d\tau. \tag{6}$$

The latter equality is valid, because the delta function is even. This formula allows $x(t)$ to be interpreted as a sum of elementary signals

$$dx(t) = x(\tau)\delta(t - \tau)d\tau. \tag{7}$$

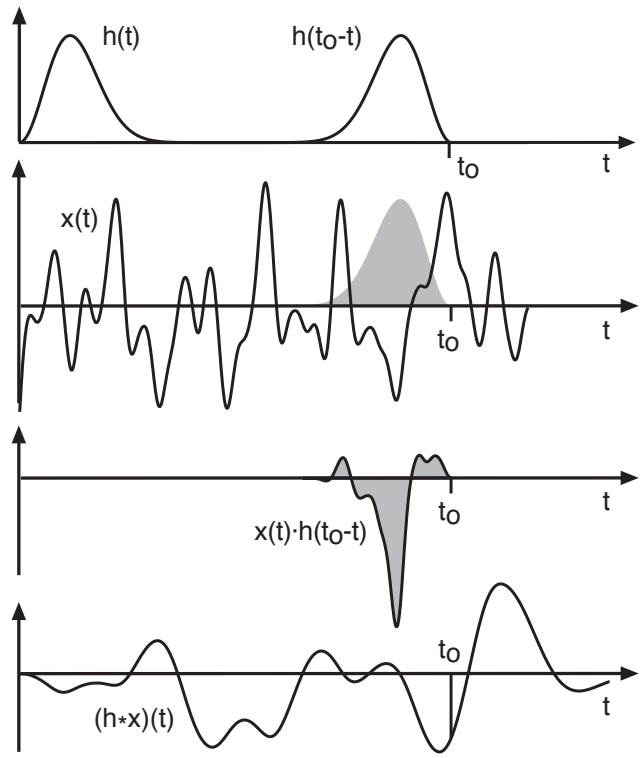

Figure 1: Convolution of input signal and impulse response.

If the input signal is $\delta(t-\tau)$, the output is obviously $h(t-\tau)$. Since the system is linear, multiplying an input by some constant also multiplies the output by the same constant. Therefore the output corresponding to an input $dx(t)$ is

$$dy(t) = x(\tau)h(t-\tau)d\tau. \tag{8}$$

Also, in a linear system the output of a sum of inputs is the sum of individual outputs of these inputs. Hence the output given by input $x(t)$ is

$$y(t) = \int_{-\infty}^{\infty} x(\tau)h(t-\tau)d\tau = (x * h)(t). \tag{9}$$

This integral is convolution, which is often briefly marked by '$*$'. Thus we have arrived at an important result: the output of a linear system is a convolution of the input and the impulse response of the system.

A Fourier transform of eq. (9) gives

$$Y(\nu) = \mathcal{F}(x) \cdot \mathcal{F}(h) = X(\nu) \cdot H(\nu), \tag{10}$$

where

$$H(\nu) = \mathcal{F}(h) = \int_{-\infty}^{\infty} h(t)e^{-i\omega t}\, dt \tag{11}$$

is the transfer function of the linear system.

This indicates that, if $H(\nu) = 0$ at some frequency range, these frequencies are filtered out in the output $y(t)$, even if the input $x(t)$ contains these frequencies.

Frequency mixing

Mixing means shifting a signal from one frequency band to another without losing its information content. Shifts to lower and higher frequency bands are also called downconversion and upconversion, respectively.

Let us consider a signal

$$x(t) = \int_{-\infty}^{\infty} X(\nu) e^{i\omega t}\, d\nu. \tag{12}$$

When $x(t)$ is real-valued, its amplitude spectrum is an even function of frequency and its phase spectrum is odd. It is always possible to write

$$X(\nu) = X^{+}(\nu) + X^{-}(\nu), \tag{13}$$

where $X^{+}(\nu) = 0$ at negative frequencies and $X^{-}(\nu) = 0$ at positive frequencies.

Multiplying $x(t)$ by $\exp(-i\omega_0 t)$ gives

$$\begin{aligned} y(t) = e^{-i\omega_0 t} x(t) = e^{-i\omega_0 t} \int_{-\infty}^{\infty} X(\nu) e^{i\omega t} d\nu &= \int_{-\infty}^{\infty} X(\nu) e^{i(\omega - \omega_0)t} d\nu \\ = \int_{-\infty}^{\infty} X(\nu + \nu_0) e^{i\omega t} d\nu &= \int_{-\infty}^{\infty} Y(\nu) e^{i\omega t} d\nu, \end{aligned} \tag{14}$$

where

$$Y(\nu) = X(\nu + \nu_0). \tag{15}$$

This shows that complex mixing shifts the whole spectrum towards negative frequencies by ν_0. With a proper choice of ν_0, $X^{+}(\nu + \nu_0)$ will lie around zero frequency in such a manner that $X^{-}(\nu + \nu_0)$ can be filtered out. The Fourier transform of the filtered signal is

$$Z(\nu) = X^{(+)}(\nu + \nu_0) \tag{16}$$

and the signal itself is

$$\begin{aligned} z(t) &= e^{-i\omega_0 t} \int_{0}^{\infty} X(\nu) e^{i\omega t} d\nu = \int_{0}^{\infty} X(\nu) e^{i(\omega - \omega_0)t} d\nu \\ &= \int_{-\nu_0}^{\infty} X(\nu + \nu_0) e^{i\omega t} d\nu. \end{aligned} \tag{17}$$

The modulus of $Z(\nu)$ is no more necessarily even and the phase odd, and therefore $z(t)$ can be a complex signal.

If, instead of $\exp(-i\omega_0 t)$, the original signal is multiplied by $\exp(i\omega_0 t)$, shifting takes place towards higher frequencies.

In radar receivers, cases also arise where frequency conversion is not made to a frequency band around zero frequency (base band). Even then the principle is the same as above.

Spectrum and autocorrelation function

Assume an experiment producing a random signal $x(t)$ each time it is carried out. Each outcome of the experiment (realisation) is different, but the signals have the same statistical properties. An example of five realisations is shown in Fig. 2. The autocorrelation function is defined by

$$R_x(t_i, t_j) = \langle x(t_i)x(t_j)\rangle = \langle x_i x_j\rangle, \tag{18}$$

where the angle brackets indicate ensemble average. If the signal is stationary, the autocorrelation function depends only on the time difference $\tau = t_i - t_j$, i.e.

$$R_x(\tau) = \langle x(t)x(t-\tau)\rangle. \tag{19}$$

Then the autocorrelation function is also obtained as a time average from a single realisation, i.e.

$$R_x(\tau) = \lim_{T\to\infty} \frac{1}{2T} \int_{-T}^{T} x(t)x(t-\tau)\, dt. \tag{20}$$

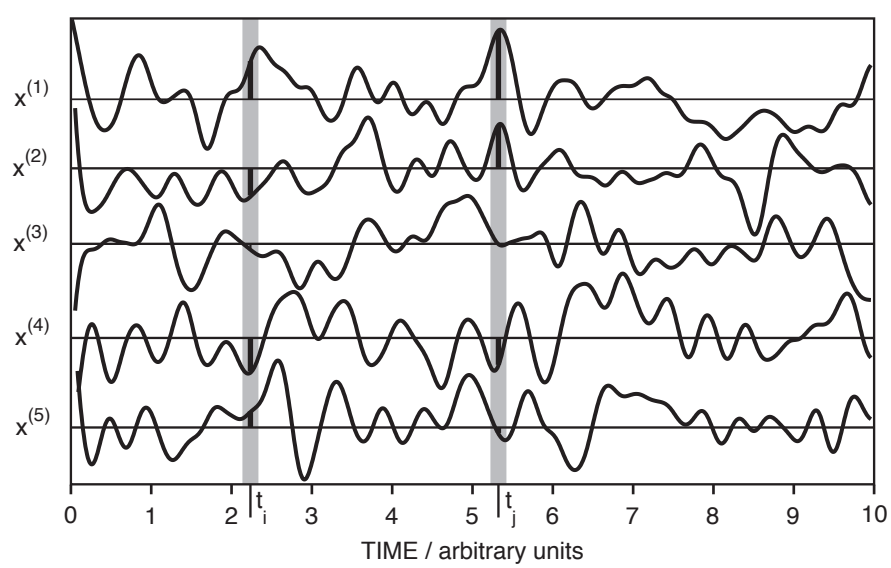

Figure 2: Realisations of a stochastic process with zero mean value.

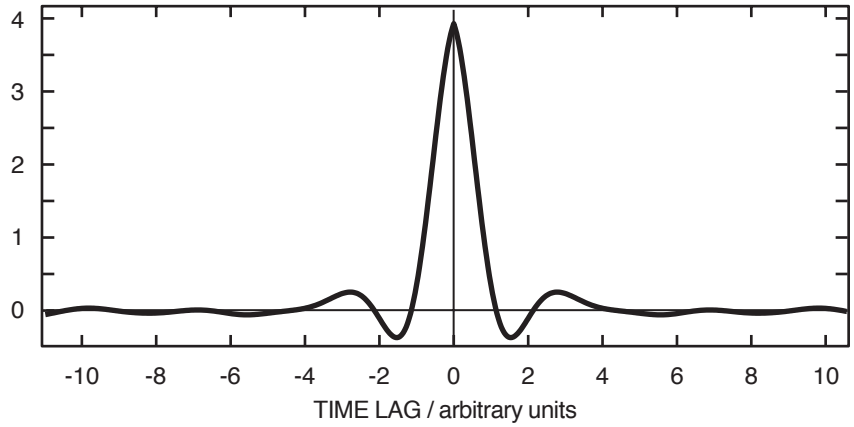

Figure 3: The autocorrelation function of the stochastic process shown in Fig. 2. The same time units are used in the two figures.

The Fourier transform of the autocorrelation function is

$$\begin{aligned} S(\nu) &= \int_{-\infty}^{\infty} R_x(\tau) e^{-i\omega\tau} d\tau = \lim_{T\to\infty} \frac{1}{2T} \int_{-T}^{T} \left[\int_{-T}^{T} x(t)x(t-\tau)\, dt \right] e^{-i\omega\tau} d\tau \\ &= \lim_{T\to\infty} \frac{1}{2T} \int_{-T}^{T} x(t) e^{-i\omega t} dt \int_{-T}^{T} x(\tau') e^{i\omega\tau'} d\tau' = \lim_{T\to\infty} \frac{1}{2T} X_T(\nu) X_T^*(\nu) \\ &= \lim_{T\to\infty} \frac{1}{2T} |X_T(\nu)|^2. \end{aligned} \tag{21}$$

Here $X_T(\nu)$ is the Fourier transform of $x(t)$ from the time interval $(-T, T)$. If $x(t)$ is voltage, the unit of autocorrelation function is V^2 (this is power for unit resistance). Then the unit of $S(\nu)$ is V^2s and the unit of $S(\nu)d\nu$ is V^2. Hence $S(\nu)$ means power per small frequency interval, i.e. $S(\nu)$ is the power spectral density of $x(t)$. Therefore the autocorrelation function and the power spectral density make a Fourier transform pair.

In the radar receiver, the signal is downconverted to a lower frequency. This is made by complex mixing and it leads to a complex signal. If $z(t)$ is a stationary complex stochastic process, the autocorrelation function must be defined as

$$R_z(\tau) = \langle z(t) z^*(t-\tau) \rangle. \tag{22}$$

Then a straightforward calculation shows that the Fourier transform of this function of the power spectrum of the signal.

Thomson scattering from a single electron

Assume electric field

$$\mathbf{E}_i = \mathbf{E}_0 e^{i\omega_0 t} \tag{23}$$

acting on an electron. The momentum equation is

$$m_e \frac{d^2\mathbf{r}_e}{dt^2} = -e\mathbf{E}_i. \tag{24}$$

This gives electron velocity

$$\mathbf{v}_e = \frac{d\mathbf{r}_e}{dt} = -\frac{e}{m_e}\int \mathbf{E}_i\, dt = -\frac{e\mathbf{E}_0}{m_e}\int e^{i\omega_0 t}\, dt = i\frac{e\mathbf{E}_0}{m_e\omega_0}e^{i\omega_0 t}. \tag{25}$$

The charge density of an electron is

$$\rho_e(\mathbf{r}, t) = -e\delta[\mathbf{r} - \mathbf{r}_e(t)] \tag{26}$$

and current density

$$\mathbf{j}(\mathbf{r}, t) = \rho_e(\mathbf{r}, t)\mathbf{v}_e(t) = -e\mathbf{v}_e(t)\cdot\delta[\mathbf{r} - \mathbf{r}_e(t)] = -i\frac{e^2\mathbf{E}_0}{m_e\omega_0}e^{i\omega_0 t}\cdot\delta[\mathbf{r} - \mathbf{r}_e(t)]. \tag{27}$$

The retarded vector potential at $\mathbf{r}$ is

$$\mathbf{A}_s(\mathbf{r}, t) = \frac{\mu_0}{4\pi}\int \frac{\mathbf{j}(\mathbf{r}', t - |\mathbf{r} - \mathbf{r}'|/c)}{|\mathbf{r} - \mathbf{r}'|}\, d^3r'. \tag{28}$$

Inserting eq. (27) in eq. (28) gives

$$\mathbf{A}_s(\mathbf{r}, t) = -i\frac{\mu_0 e^2\mathbf{E}_0}{4\pi m_e\omega_0}\int \frac{e^{i\omega_0(t-|\mathbf{r}-\mathbf{r}'|/c)}}{|\mathbf{r}-\mathbf{r}'|}\cdot\delta[\mathbf{r}'-\mathbf{r}_e(t - |\mathbf{r}-\mathbf{r}'|/c)]\, d^3r'. \tag{29}$$

Put the electron oscillating around the origin. Far from the origin $\mathbf{r} \gg \mathbf{r}_e \approx 0$ and

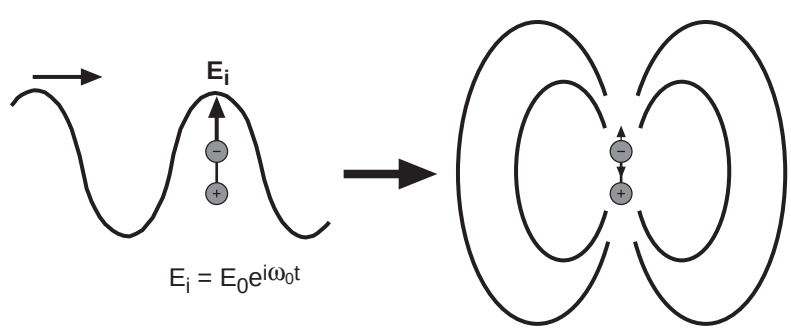

Figure 4: The mechanism of Thomson scattering in terms of dipole radiation of an oscillating electron.

$$\mathbf{A}_s(\mathbf{r},t) = -i\frac{\mu_0 e^2 \mathbf{E}_0}{4\pi m_e \omega_0} \cdot \frac{e^{i\omega_0\,(t - r/c)}}{r}. \tag{30}$$

The wave vector in the direction of $\mathbf{r}$ is

$$\mathbf{k}_s = \frac{\omega_0}{c}\mathbf{e}_s \quad \text{where} \quad \mathbf{e}_s = \frac{\mathbf{r}}{r}. \tag{31}$$

Then

$$\mathbf{A}_s(\mathbf{r},t) = -i\frac{\mu_0 e^2 \mathbf{E}_0}{4\pi m \omega_0} \cdot \frac{e^{i(\omega_0 t - \mathbf{k}_s \cdot \mathbf{r})}}{r}. \tag{32}$$

Far from the origin the wave fronts are nearly planes. Therefore

$$\nabla\times \approx -i\mathbf{k}_s\times$$

and the magnetic induction of the scattered wave is

$$\mathbf{B}_s = \nabla \times \mathbf{A}_s \approx -\frac{\mu_0 e^2 (\mathbf{k}_s \times \mathbf{E}_0)}{4\pi m_e \omega_0} \cdot \frac{e^{i(\omega_0 t - \mathbf{k}_s \cdot \mathbf{r})}}{r}. \tag{33}$$

The electric field of the scattered wave is

$$\mathbf{E}_s = c\mathbf{B}_s \times \mathbf{e}_s. \tag{34}$$

Then the electric field of the scattered wave is

$$\mathbf{E}_s = \frac{c\mu_0 e^2 k_s E_0 \sin\mathcal{X}}{4\pi m_e \omega_0} \cdot \frac{e^{i(\omega_0 t - \mathbf{k}_s \cdot \mathbf{r})}}{r}\mathbf{e}_\perp = r_e E_0 \sin\mathcal{X} \cdot \frac{e^{i(\omega_0 t - \mathbf{k}_s \cdot \mathbf{r})}}{r}\mathbf{e}_\perp, \tag{35}$$

where the electron classical radius is

$$r_e = \frac{c\mu_0 e^2 k_s}{4\pi m_e \omega_0} = \frac{\mu_0 e^2}{4\pi m_e} = \frac{e^2}{4\pi\varepsilon_0 m_e c^2} = 2.82 \cdot 10^{-15}\,\mathrm{m} \tag{36}$$

and

$$\mathbf{e}_\perp = \frac{\mathbf{e}_s \times (\mathbf{e}_s \times \mathbf{E}_0)}{E_0} \tag{37}$$

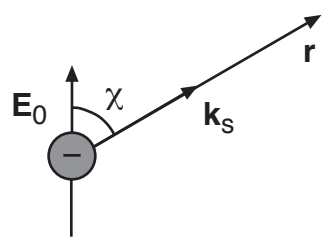

Figure 5: The angle between the electric field of the incident wave and the scattering direction.

Scattering from density fluctuations

The displacement vector due to an electric field $\mathbf{E}$ is

$$\mathbf{D} = \varepsilon\varepsilon_0\mathbf{E} = \varepsilon_0\mathbf{E} + \mathbf{P}, \tag{38}$$

where $\mathbf{P}$ is the volume polarisation

$$\mathbf{P} = (\varepsilon - 1)\varepsilon_0\mathbf{E}. \tag{39}$$

The permittivity is a sum of its average value and fluctuation

$$\varepsilon(\mathbf{r}, t) = \langle\varepsilon\rangle + \Delta\varepsilon(\mathbf{r}, t), \tag{40}$$

Then

$$\mathbf{P} = (\langle\varepsilon\rangle + \Delta\varepsilon - 1)\varepsilon_0\mathbf{E} = (\langle\varepsilon\rangle - 1)\varepsilon_0\mathbf{E} + \Delta\varepsilon \cdot \varepsilon_0\mathbf{E} = \mathbf{P}_{\langle\varepsilon\rangle} + \Delta\mathbf{P}. \tag{41}$$

Hence the polarisation fluctuation is

$$\Delta\mathbf{P} = \Delta\varepsilon \cdot \varepsilon_0\mathbf{E}. \tag{42}$$

Volume polarisation creates polarisation current density

$$\mathbf{j}_P = \frac{\partial\mathbf{P}}{\partial t} = \frac{\partial(\Delta\mathbf{P})}{\partial t} = \Delta\varepsilon\varepsilon_0\frac{\partial\mathbf{E}}{\partial t}. \tag{43}$$

This current density emits radiation, i.e. it is responsible for scattering.

In Fig. 6, a small scattering volume δV within the crossing of the two antenna beams is considered. Here $\mathbf{r}_s$ indicates the centre of δV. The electric field of the transmitted spherical wave at $\mathbf{r}$ can be written as

$$\mathbf{E} = \mathbf{E}_0(\mathbf{r})e^{i(\omega_0 t - k_0 r)}. \tag{44}$$

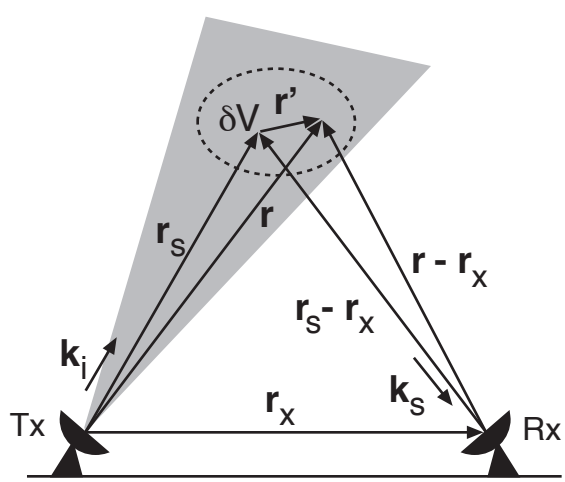

Figure 6: Scattering from a small volume δV.

It causes a polarisation fluctuation

$$\Delta\mathbf{P} = \Delta\varepsilon(\mathbf{r},t)\varepsilon_0\mathbf{E}_0(\mathbf{r})e^{i(\omega_0 t - k_0 r)}, \tag{45}$$

and a polarisation current density

$$\mathbf{j}_P = \frac{\partial(\Delta\mathbf{P})}{\partial t} = i\omega_0\Delta\varepsilon(\mathbf{r},t)\varepsilon_0\mathbf{E}_0(\mathbf{r})e^{i(\omega_0 t - k_0 r)}. \tag{46}$$

The current within a volume element d^3r (inside δV) causes a vector potential

$$d\mathbf{A}_s = \frac{\mu_0}{4\pi}\cdot\frac{\mathbf{j}_P\, d^3r}{|\mathbf{r}-\mathbf{r}_x|} \tag{47}$$

at the receiver. The retarded vector potential at $\mathbf{r}_x$ is

$$\begin{aligned} d\mathbf{A}_s(\mathbf{r}_x,t) &= \frac{\mu_0}{4\pi}\cdot\frac{\mathbf{j}_P\left(\mathbf{r},t-|\mathbf{r}-\mathbf{r}_x|/c\right)}{|\mathbf{r}-\mathbf{r}_x|}d^3r \\ &= \frac{i\omega_0\mu_0\varepsilon_0\mathbf{E}_0(\mathbf{r})\Delta\varepsilon\left(\mathbf{r},t-|\mathbf{r}-\mathbf{r}_x|/c\right)}{4\pi|\mathbf{r}-\mathbf{r}_x|}e^{i[\omega_0 t - k_0(r+|\mathbf{r}-\mathbf{r}_x|)]}d^3r. \end{aligned} \tag{48}$$

The dimensions of δV are much smaller than its distance from the transmitter or the receiver. Then

$$\mathbf{E}_0(\mathbf{r}) \approx \mathbf{E}_0(\mathbf{r}_s). \tag{49}$$

Also, for the denominator of eq. (48) and the slowly varying $\Delta\varepsilon$

$$|\mathbf{r}-\mathbf{r}_x| \approx |\mathbf{r}_s-\mathbf{r}_x|. \tag{50}$$

This approximation is not valid for the fast varying exponential. In order to approximate the exponential we use a definition

$$\mathbf{r}' = \mathbf{r}-\mathbf{r}_s. \tag{51}$$

Then

$$|\mathbf{r}-\mathbf{r}_x| \approx |\mathbf{r}_s-\mathbf{r}_x| + \mathbf{r}'\cdot\frac{(\mathbf{r}_s-\mathbf{r}_x)}{|\mathbf{r}_s-\mathbf{r}_x|} \tag{52}$$

and

$$r \approx r_s + \frac{\mathbf{r}'\cdot\mathbf{r}_s}{r_s}. \tag{53}$$

These approximations give

$$\begin{aligned} k_0(r+|\mathbf{r}-\mathbf{r}_x|) &= k_0\left[r_s + \mathbf{r}'\cdot\frac{\mathbf{r}_s}{r_s} + |\mathbf{r}_s-\mathbf{r}_x| + \mathbf{r}'\cdot\frac{(\mathbf{r}_s-\mathbf{r}_x)}{|\mathbf{r}_s-\mathbf{r}_x|}\right] \\ &= \mathbf{k}_i\cdot\mathbf{r}_s + \mathbf{k}_i\cdot\mathbf{r}' + \mathbf{k}_s\cdot(\mathbf{r}_x-\mathbf{r}_s) - \mathbf{k}_s\cdot\mathbf{r}'. \end{aligned} \tag{54}$$

where

$$\mathbf{k}_i = k_0\frac{\mathbf{r}_s}{r_s} \quad \text{and} \quad \mathbf{k}_s = k_0\frac{\mathbf{r}_x-\mathbf{r}_s}{|\mathbf{r}_x-\mathbf{r}_s|}. \tag{55}$$

Then

$$d\mathbf{A}_s(\mathbf{r}_x,t) = \frac{i\omega_0\mu_0\varepsilon_0\mathbf{E}_0(\mathbf{r}_s)}{4\pi|\mathbf{r}_s-\mathbf{r}_x|}\exp\{i[\omega_0 t-\mathbf{k}_i\cdot\mathbf{r}_s-\mathbf{k}_s\cdot(\mathbf{r}_x-\mathbf{r}_s)]\}\Delta\varepsilon\,(\mathbf{r}',t')\,e^{-i(\mathbf{k}_i\,-\,\mathbf{k}_s)\,\cdot\,\mathbf{r}'}d^3r'. \tag{56}$$

The total vector potential scattered from all elements inside δV contains the integral

$$\int\limits_{\delta V}\Delta\varepsilon(\mathbf{r}',t')e^{-i(\mathbf{k}_i\,-\,\mathbf{k}_s)\,\cdot\,\mathbf{r}'}d^3r'. \tag{57}$$

This is obviously the three-dimensional spatial Fourier transform of $\Delta\varepsilon$

$$\Delta\mathcal{E}(\mathbf{k},t) = \int\Delta\varepsilon(\mathbf{r},t)\,e^{-i\mathbf{k}\,\cdot\,\mathbf{r}}\,d^3r \tag{58}$$

calculated at a wave number $\mathbf{k}=\mathbf{k}_i-\mathbf{k}_s$. The total vector potential at the receiver is

$$\delta\mathbf{A}_s(\mathbf{r}_x,t) = \frac{i\omega_0\mu_0\varepsilon_0\mathbf{E}_0(\mathbf{r}_s)}{4\pi|\mathbf{r}_s-\mathbf{r}_x|}|\Delta\mathcal{E}(\mathbf{k}_i-\mathbf{k}_s,t)|\exp\{i[\omega_0 t-\mathbf{k}_i\cdot\mathbf{r}_s-\mathbf{k}_s\cdot(\mathbf{r}_x-\mathbf{r}_s)+\varphi_\varepsilon]\}, \tag{59}$$

where φ_ε is the phase of $\Delta\mathcal{E}$. The magnetic induction of the scattered radiation is

$$\delta\mathbf{B}_s(\mathbf{r}_x,t) = \frac{\omega_0\mu_0\varepsilon_0\mathbf{k}_s\times\mathbf{E}_0(\mathbf{r}_s)}{4\pi|\mathbf{r}_s-\mathbf{r}_x|}|\Delta\mathcal{E}(\mathbf{k}_i-\mathbf{k}_s,t)|\exp\{i[\omega_0 t-\mathbf{k}_i\cdot\mathbf{r}_s-\mathbf{k}_s\cdot(\mathbf{r}_x-\mathbf{r}_s)+\varphi_\varepsilon]\} \tag{60}$$

and the scattered electric field is $\mathbf{E}_s = c\mathbf{B}_s\times\mathbf{e}_s$, i.e.

$$\delta\mathbf{E}_s(\mathbf{r}_x,t) = \frac{\omega_0^2E_0(\mathbf{r}_s)\sin\mathcal{X}}{4\pi c^2|\mathbf{r}_s-\mathbf{r}_x|}|\Delta\mathcal{E}(\mathbf{k}_i-\mathbf{k}_s,t)|\exp\{i[\omega_0 t-\mathbf{k}_i\cdot\mathbf{r}_s-\mathbf{k}_s\cdot(\mathbf{r}_x-\mathbf{r}_s)+\varphi_\varepsilon]\}\,\mathbf{e}_\perp. \tag{61}$$

This applies to all cases where scattering takes place at permittivity fluctuations, whatever the reason for the fluctuations may be. In plasma, the refractive index is

$$n = \sqrt{1-\frac{n_e e^2}{\varepsilon_0 m_e\omega_0^2}}. \tag{62}$$

Here n_e is the electron density, e is the (positive) elementary charge and m_e is the electron mass. Thus the plasma permittivity is

$$\varepsilon = n^2 = 1-\frac{n_e e^2}{\varepsilon_0 m_e\omega_0^2}. \tag{63}$$

This indicates that the permittivity and electron density fluctuations $\Delta\varepsilon$ and Δn_e are connected by

$$\Delta\varepsilon = -\frac{e^2}{\varepsilon_0 m_e\omega_0^2}\cdot\Delta n_e. \tag{64}$$

and consequently,

$$\Delta\mathcal{E} = -\frac{e^2}{\varepsilon_0 m_e\omega_0^2}\cdot\Delta N_e, \tag{65}$$

where ΔN_e is the spatial Fourier transform of Δn_e. Then, using the definition of the classical electron radius (36), eq. (61) can be written as

$$\delta E_s(\mathbf{r}_x, t) = \frac{r_e \sin \mathcal{X}}{|\mathbf{r}_s - \mathbf{r}_x|} |\Delta N_e(\mathbf{k}_i - \mathbf{k}_s, t)| E_0(\mathbf{r}_s) \exp\{i[\omega_0 t - \mathbf{k}_i \cdot \mathbf{r}_s - \mathbf{k}_s \cdot (\mathbf{r}_x - \mathbf{r}_s) + \varphi_N]\}. \quad (66)$$

This is the elementary signal from elementary volume δV.

In the receiver, the signal is amplified and downconverted. The resulting complex voltage is

$$\delta z(t) = (RP_0)^{1/2} |\Delta N_e(\mathbf{k}_i - \mathbf{k}_s, t)| e^{i\varphi_N} e^{i\varphi} = (RP_0)^{1/2} \Delta N_e(\mathbf{k}_i - \mathbf{k}_s, t) e^{i\varphi}. \quad (67)$$

Here φ is a phase, R is the receiver impedance and P_0 is a power coefficient

$$P_0 \propto \frac{r_e^2 \sin^2 \mathcal{X}}{|\mathbf{r}_s - \mathbf{r}_x|^2}, \quad (68)$$

which depends on

- transmitted power
- distance from scattering volume to receiver
- antenna gains
- receiver amplification.

Scattering from wave fronts

The density fluctuation is

$$\Delta n_e(\mathbf{r}, t) = n_e(\mathbf{r}, t) - n_{e0} \quad (69)$$

and its three-dimensional spatial Fourier transform is

$$\Delta N_e(\mathbf{k}, t) = \iiint_{-\infty}^{\infty} \Delta n_e(\mathbf{r}, t) e^{-i\mathbf{k} \cdot \mathbf{r}} \, d^3 r, \quad (70)$$

so that

$$\Delta n_e(\mathbf{r}, t) = \frac{1}{(2\pi)^3} \iiint_{-\infty}^{\infty} \Delta N_e(\mathbf{k}, t) e^{i\mathbf{k} \cdot \mathbf{r}} \, d^3 k. \quad (71)$$

Also, the temporal Fourier transform of $\Delta N_e(\mathbf{k}, t)$ is

$$\mathcal{N}_e(\mathbf{k}, \nu) = \int_{-\infty}^{\infty} \Delta N_e(\mathbf{k}, t) e^{-i\omega t} \, dt \quad (72)$$

so that

$$\Delta N_e(\mathbf{k}, t) = \int_{-\infty}^{\infty} \mathcal{N}_e(\mathbf{k}, \nu) e^{i\omega t} \, d\nu. \quad (73)$$

Inserting this in eq. (71) gives

$$\begin{aligned}\Delta n_e(\mathbf{r},t) &= \frac{1}{(2\pi)^3}\iiint\limits_{-\infty}^{\infty}\left[\int\limits_{-\infty}^{\infty}\mathcal{N}_e(\mathbf{k},\nu)e^{i\omega t}\,d\nu\right]e^{i\mathbf{k}\cdot\mathbf{r}}\,d^3k \\ &= \frac{1}{(2\pi)^3}\iiint\limits_{-\infty}^{\infty}\left[\int\limits_{-\infty}^{\infty}\mathcal{N}_e(\mathbf{k},\nu)e^{i(\omega t+\mathbf{k}\cdot\mathbf{r})}\,d\nu\right]d^3k. \qquad (74)\end{aligned}$$

Hence the density fluctuation is composed of waves propagating in all directions.

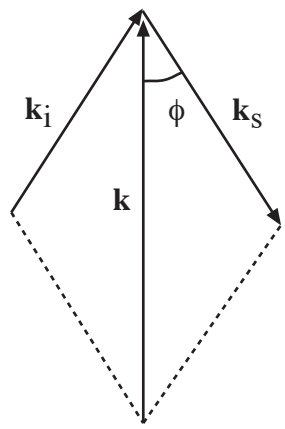

Figure 7: The relation of incident and scattered wave vectors and the wave vector of the permittivity fluctuation.

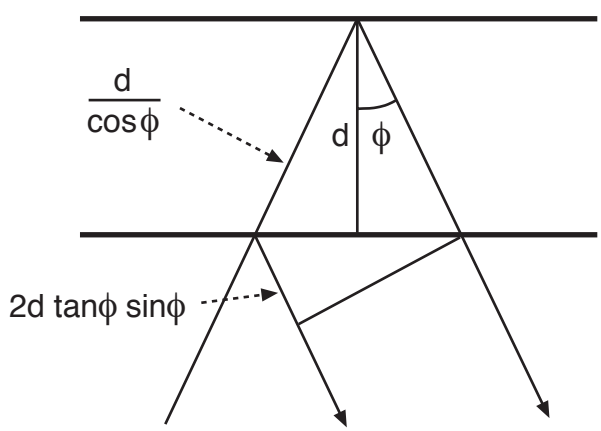

Figure 8: Scattering from parallel wave fronts.

This can be visualised as follows. It was shown above that scattering is due to the Fourier component $\Delta N_e(\mathbf{k}_i-\mathbf{k}_s,t)$, i.e. at a wave number $\mathbf{k}=\mathbf{k}_i-\mathbf{k}_s$. Since $k_i=k_s=k_0=2\pi/\lambda_0$,

$k = 2k_0 \cos\phi$ and the corresponding wave length is

$$\lambda = \frac{\lambda_0}{2\cos\phi}. \tag{75}$$

If the radio waves were scattered from parallel wave fronts separated by a distance d, their path difference would be

$$\Delta = \frac{2d}{\cos\phi} - 2d\tan\phi\sin\phi = 2d\cos\phi. \tag{76}$$

Constructive interference is given by

$$d = \frac{\lambda_0}{2\cos\phi}. \tag{77}$$

The distance in eq. (77) is equal to the wave length λ in eq. (75).

The two main wave modes contributing to density fluctuations are

1. Ion acoustic waves
2. Langmuir waves

Ion acoustic waves are non-dispersive. Their phase velocity is

$$v_\oplus = \sqrt{\frac{k_B(T_i + T_e)}{m_i}}. \tag{78}$$

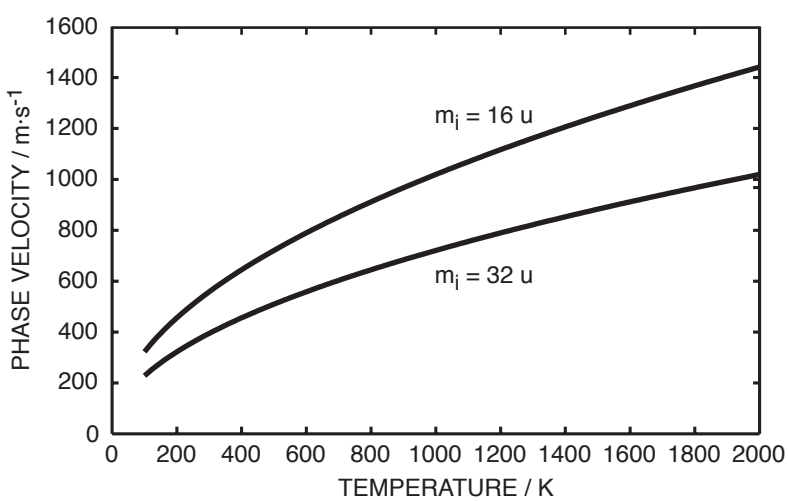

Figure 9: Phase velocity of ion acoustic wave for O^+ and O_2^+ ions as a function of temperature. Equal ion and electron temperatures are assumed.

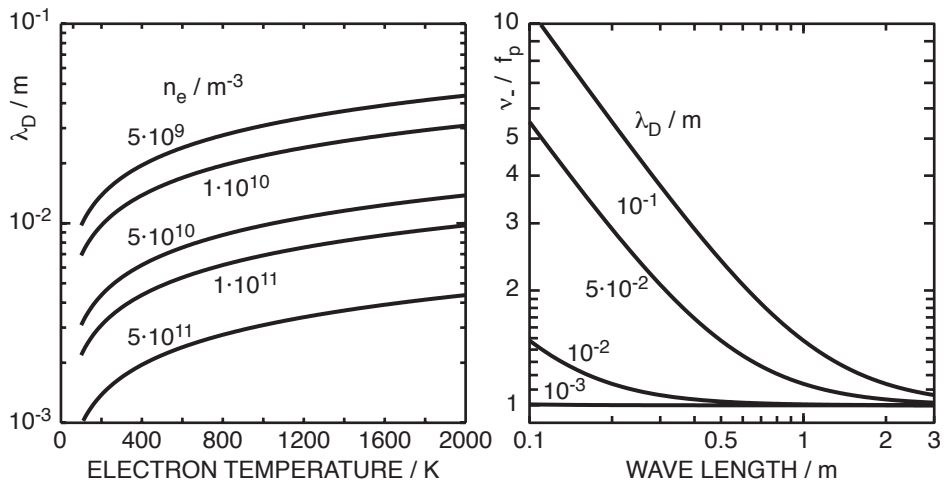

Figure 10: Left hand panel: Debye length as a function of electron temperature for different values of electron density. Right hand panel: The frequency of Langmuir wave (normalised by plasma frequency) as a function of wave length for different values of Debye length.

Langmuir waves are dispersive and they are excited by energetic electrons. Their phase velocity is

$$v_\ominus = \lambda_\ominus \cdot f_p \sqrt{1 + 12\pi^2 \lambda_D^2 / \lambda_\ominus^2}, \tag{79}$$

where $\lambda_\ominus$ is the wave length,

$$f_p = \frac{1}{2\pi} \left[\frac{n_e e^2}{\varepsilon_0 m_e} \right]^{1/2} \tag{80}$$

is the plasma frequency and

$$\lambda_D = \left[\frac{\varepsilon_0 k_B T_e}{n_e e^2} \right]^{1/2} \tag{81}$$

is the Debye length.
Since the plasma waves are in motion, the scattered waves are Doppler shifted. The sacttering electrons in the moving wave fronts experience a Doppler-shifted frequency

$$\nu' = \nu_0 \sqrt{\frac{c + v_\perp \mathbf{e}_\perp \cdot \mathbf{e}_T}{c - v_\perp \mathbf{e}_\perp \cdot \mathbf{e}_T}}. \tag{82}$$

At the receiver, after a second Doppler shift, the observed frequency is

$$\nu'' = \nu' \sqrt{\frac{c + v_\perp \mathbf{e}_\perp \cdot \mathbf{e}_R}{c - v_\perp \mathbf{e}_\perp \cdot \mathbf{e}_T}} = \nu_0 \sqrt{\frac{(c + v_\perp \mathbf{e}_\perp \cdot \mathbf{e}_R)(c + v_\perp \mathbf{e}_\perp \cdot \mathbf{e}_R)}{(c - v_\perp \mathbf{e}_\perp \cdot \mathbf{e}_T)(c - v_\perp \mathbf{e}_\perp \cdot \mathbf{e}_T)}}. \tag{83}$$

Since $\mathbf{e}_\perp \cdot \mathbf{e}_T = \mathbf{e}_\perp \cdot \mathbf{e}_R = \cos\phi$, this can be written as

$$\nu'' = \nu_0 \frac{c + v_\perp \cos\phi}{c - v_\perp \cos\phi} \approx \nu_0 \left(1 + 2 \frac{v_\perp \cos\phi}{c} \right). \tag{84}$$

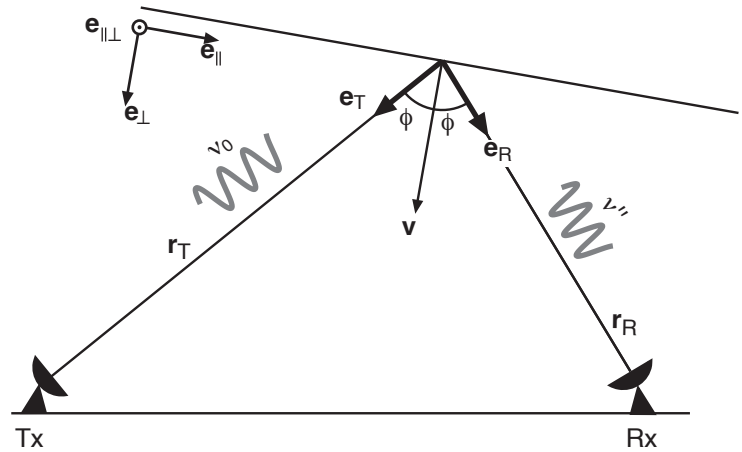

Figure 11: Generation of Doppler shift in scattering from plasma waves.

Then the observed Doppler shift is

$$\delta\nu = \nu'' - \nu_0 = 2\nu_0 \frac{v_\perp \cos\phi}{c} = 2\frac{v_\perp \cos\phi}{\lambda_0}. \tag{85}$$

Since $\lambda_0 = 2\lambda\cos\phi$, we can also write

$$\delta\nu = 2\frac{v_\perp \cos\phi}{2\lambda\cos\phi} = \frac{v_\perp}{\lambda}. \tag{86}$$

This frequency shift is given by the frequency of the plasma fluctuation at a wave length $\lambda = \lambda_0/(2\cos\phi)$. The result is valid separately for ion acoustic waves and Langmuir waves. Thus the scattering spectrum should contain four lines, two of them caused by ion acoustic waves and two by Langmuir waves. These are called ion lines and plasma lines, respectively, and they are shown schematically in Fig. 12.

Since the phase velocity of the ion acoustic wave is independent of wave length, it is convenient to use eq. (85) in calculating the Doppler shift of the ion lines. This gives

$$\delta\nu_i = \pm 2\frac{v_\oplus \cos\phi}{\lambda_0}, \tag{87}$$

indicating that the frequency shift depends on the angle ϕ. The maximum Doppler shift $2v_\oplus/\lambda_0$ is observed in backscattering. When the radar wave length is 0.3–1.5 m and the phase velocity a few hundreds of metres per second, the Doppler shift is of the order of a few kilohertz or even less.

The Doppler shift of plasma lines can be calculated from eqs. (86) and (79), and the result is

$$\delta\nu_p = \pm\frac{v_\ominus}{\lambda_\ominus} = \pm f_p\sqrt{1 + 48\pi^2\lambda_D^2\cos^2\phi/\lambda_0^2}. \tag{88}$$

Fig. 10 reveals that, for typical values of Debye length in the ionosphere, the frequency of the Langmuir wave is quite close to the plasma frequency (e.g. for $\lambda_D = 5$ mm, $\lambda_0 = 32$ cm

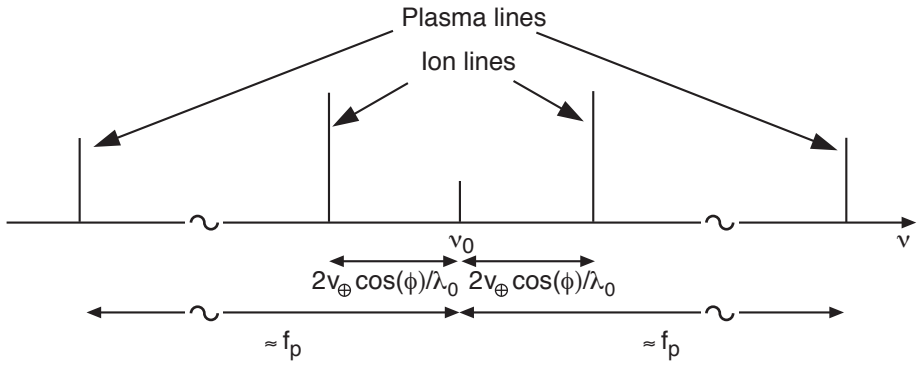

Figure 12: Location of ion and plasma lines around the transmitter frequency.

and $\phi = 0$, eq. (88) gives $\nu_{\ominus} = 1.06 f_p$). Hence the Debye term in eq. (88) is small as compared to unity and the Doppler shift is independent of ϕ in practice. Eq. (88) also means that the Doppler shift is typically of the order of several megahertz, i.e. the plasma lines lie about three orders of magnitude further from the transmitter frequency than the ion lines do.

In the above discussion a zero bulk plasma motion was assumed. If the plasma is moving in the radar frame of reference, the theory must be modified to include an additional Doppler shift. In Fig. 13 the ionospheric plasma is in motion and its bulk velocity is

$$\mathbf{u} = u_{\|}\mathbf{e}_{\|} + u_{\perp}\mathbf{e}_{\perp} + u_{\|\perp}\mathbf{e}_{\|\perp}.$$

The component of $\mathbf{v}_e$ in the direction of the transmitter beam is $\mathbf{v}_e \cdot \mathbf{e}_T$. The electrons

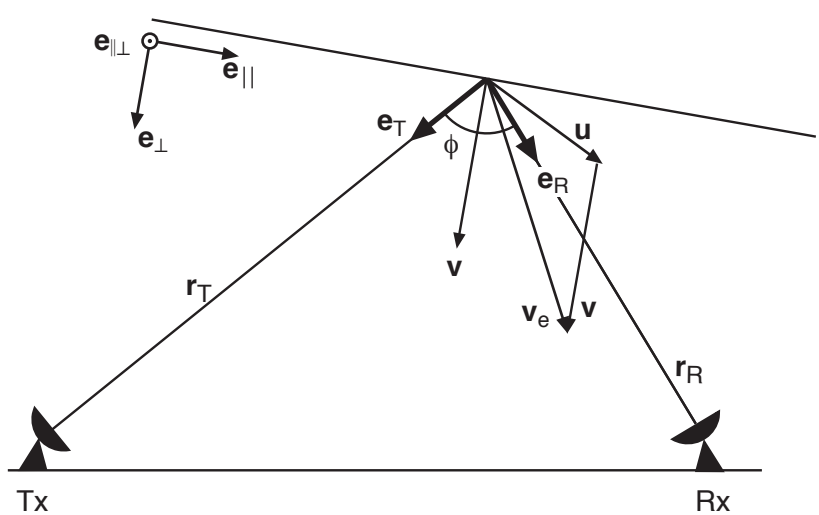

Figure 13: The effect of plasma flow on Doppler shift.

observe the transmitted wave at a frequency

$$\nu' = \nu_0 \sqrt{\frac{c + \mathbf{v}_e \cdot \mathbf{e}_T}{c - \mathbf{v}_e \cdot \mathbf{e}_T}} \tag{89}$$

and the frequency observed at the receiver is

$$\nu'' = \nu' \sqrt{\frac{c + \mathbf{v}_e \cdot \mathbf{e}_R}{c - \mathbf{v}_e \cdot \mathbf{e}_R}} = \nu_0 \sqrt{\frac{(c + \mathbf{v}_e \cdot \mathbf{e}_T)(c + \mathbf{v}_e \cdot \mathbf{e}_R)}{(c - \mathbf{v}_e \cdot \mathbf{e}_T)(c - \mathbf{v}_e \cdot \mathbf{e}_R)}}. \tag{90}$$

Using $\mathbf{v} = v_\perp \mathbf{e}_\perp$ and $\mathbf{u} = u_\parallel \mathbf{e}_\parallel + u_\perp \mathbf{e}_\perp + u_{\parallel\perp} \mathbf{e}_{\parallel\perp}$ and, noticing that $\mathbf{e}_{\parallel\perp} \cdot \mathbf{e}_T = \mathbf{e}_{\parallel\perp} \cdot \mathbf{e}_R = 0$, this can be put in the form

$$\nu'' = \nu_0 \sqrt{\frac{[c + (v + u_\perp)\cos\phi]^2 - u_\parallel^2 \sin^2\phi}{[c - (v + u_\perp)\cos\phi]^2 - u_\parallel^2 \sin^2\phi}}. \tag{91}$$

Since $u_\parallel^2 \sin^2\phi$ is small in comparison with the other term, it can be neglected. Then

$$\nu'' = \nu_0 \frac{c + (v_\perp + u_\perp)\cos\phi}{c - (v_\perp + u_\perp)\cos\phi} \approx \nu_0 \left[1 + 2\frac{(v_\perp + u_\perp)\cos\phi}{c}\right], \tag{92}$$

and the total Doppler shift is

$$\delta\nu = \nu'' - \nu_0 = 2\nu_0 \frac{(v_\perp + u_\perp)\cos\phi}{c}, \tag{93}$$

and the Doppler shift due to the bulk plasma motion is

$$\delta\nu_u = 2\nu_0 \frac{u_\perp \cos\phi}{c}. \tag{94}$$

This allows the measurement of the plasma velocity.

Plasma autocorrelation function and incoherent scatter spectrum

The autocorrelation function of the radar signal in eq. (67) is

$$\langle \delta z(\mathbf{r},t)\delta z^*(\mathbf{r},t')\rangle = RP_0\langle \Delta N_e(\mathbf{k}_i-\mathbf{k}_s,t)\Delta N_e^*(\mathbf{k}_i-\mathbf{k}_s,t')\rangle. \tag{95}$$

If the statistical properties of the plasma inside the elementary volume $\delta V(\mathbf{r})$ are constant, $\delta z(\mathbf{r},t)$ is a stationary stochastic process and it is possible to define the plasma autocorrelation function

$$\sigma_e(\mathbf{r},t-t') = \langle \Delta N_e(\mathbf{k}_i-\mathbf{k}_s,t)\Delta N_e^*(\mathbf{k}_i-\mathbf{k}_s,t')\rangle. \tag{96}$$

Then the autocorrelation function of an elementary signal from $\delta V(\mathbf{r})$ is given by

$$\langle \delta z(\mathbf{r},t)\delta z^*(\mathbf{r},t')\rangle = RP_0\sigma_e(\mathbf{r},t-t'). \tag{97}$$

The power spectrum of the scattering signal is

$$\delta S(\nu) = RP_0\int_{-\infty}^{\infty}\sigma_e(\tau)e^{-i\omega\tau}d\tau = RP_0\Sigma_e(\nu), \tag{98}$$

where

$$\Sigma_e(\nu) = \int_{-\infty}^{\infty}\sigma_e(\tau)e^{-i\omega\tau}d\tau \tag{99}$$

is the scattering spectrum.
It was stated above that the scattering spectrum consists of two plasma lines and two ion lines. This is an oversimplification. The ion lines are broadened by damping of the ion acoustic waves. Damping takes place due to ion-neutral collisions but, even in the absence of collisions, due to Landau damping. Landau damping results from the velocity distribution of ions, and Vlasov equation is needed for its theoretical treatment. The principle, however, can be understood in a simple way.

Assume a pulse of molecules (top panel) with no thermal velocities travelling at some bulk velocity. The shape of the pulse does not change.

When the molecules have a thermal velocity distribution, some molecules travel faster and some slower than the pulse. The amount depends on the thermal velocities of individual molecules (middle panel).

The result is that the pulse gradually disintegrates (bottom panel).

This is a diffusion like process which is also going on in ion acoustic waves which contain density gradients. It causes damping of the wave, even when no ion-neutral collisions are present.

The broadening due to Landau damping can be understood as follows. The power spectrum and the plasma autocorrelation function of a signal are connected by Fourier transform. The autocorrelation function of a sinusoidal ion acoustic wave is also sinusoidal

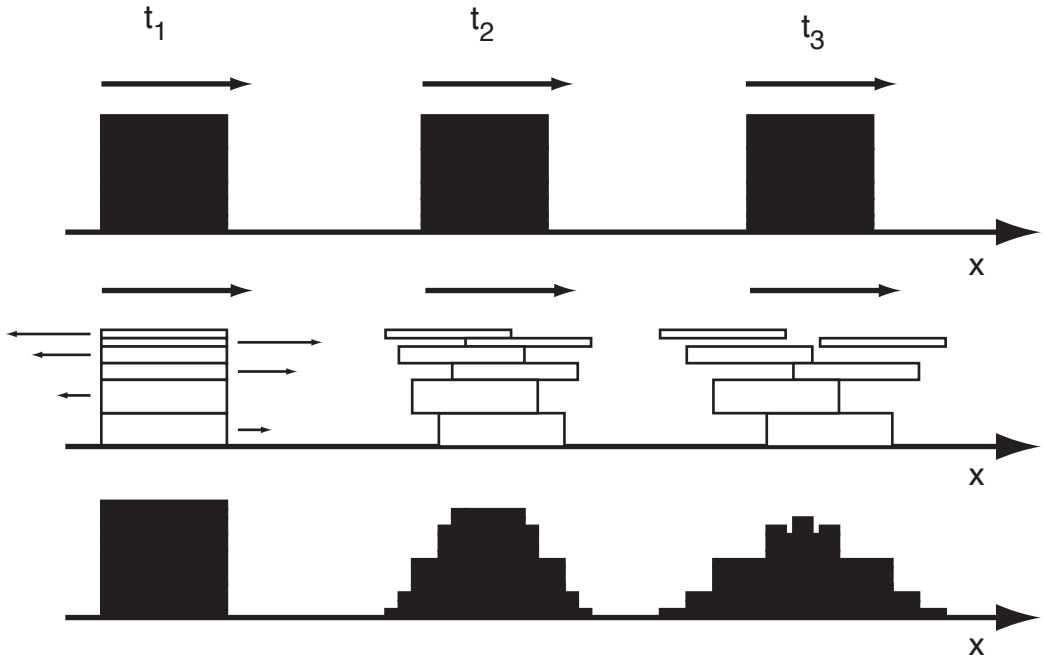

Figure 14: The principle of Landau damping.

and the power spectrum is a delta peak. However, all the time ion acoustic waves are thermally generated as well as attenuated in the plasma. Therefore the amplitude and

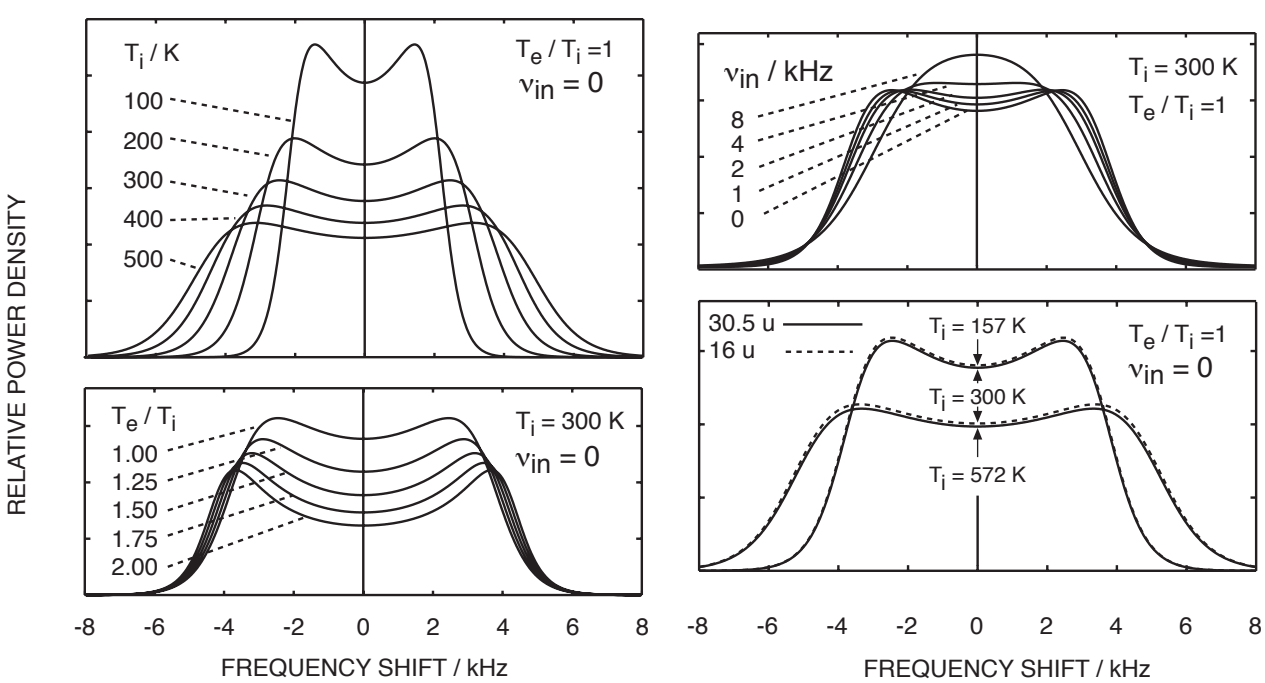

Figure 15: Dependence of ion line shape on plasma parameters

phase of a given Fourier component at a sufficiently distant time in the past have no relation to the the present amplitude and phase whatsoever. In terms of autocorrelation function, this means that the autocorrelation function of the scattered signal is attenuated with increasing delay. Then the autocorrelation function is no more sinusoidal and the corresponding spectrum can no more be a delta function but it must be broader. It turns out that Landau damping is so heavy that the two ion lines merge into a single line.

The shape of the ion line depends on ion and electron temperatures, ion-neutral collision frequency and ion mass:

Correlation of incoherent scatter signal

For investigating the spectrum and autocorrelation function of the incoherent scatter signal, we must find an elementary signal from an elementary volume. The volume must be such that signals from different parts of it are not statistically independent. Consider bistatic radar.

- Ellipsoid is a surface which reflects rays from one focal point to the other focal point.
- Density fluctuation can be built of elliptic wave fronts with transmitter and receiver at the two focal points of the ellipsoid.
- Ion acoustic waves are heavily damped; typically at distances of the order of a single wave length.
- Scattering takes place at thin shells with an ellipsoid shape.
- Correlating signals can only obtained from regions of the ellipsoid which are equidistant from the transmitter, thus a thin stripe cut from an elliptic shell could work as an elementary volume giving an elementary scattering signal.

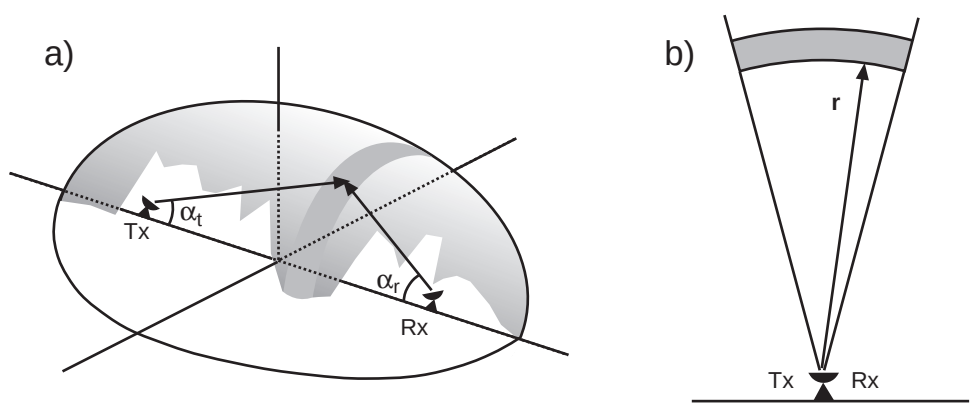

Figure 16: Scattering from from elliptic and spherical wave fronts.

- The antenna beam cuts a piece of this stripe. This is the elementary volume δV producing a coherent scattering signal in the receiver.
- In the case of a monostatic radar, spherical wave fronts of plasma waves should be considered. Then the flight time from transmitter to each point of the wave front is the same. Hence the elementary volume δV is obtained by cutting a piece from a spherical thin shell.

Consider lementary signals $\delta z_1(\mathbf{r}_1, t)$ and $\delta z_2(\mathbf{r}_2, t)$ from two elementary volumes δV_1 and δV_2, located at $\mathbf{r}_1$ and $\mathbf{r}_2$. The sum signal is

$$\delta z(\mathbf{r}_1, \mathbf{r}_2, t) = \delta z_1(\mathbf{r}_1, t) + \delta z_2(\mathbf{r}_2, t). \tag{100}$$

The autocorrelation function of this signal is

$$\begin{aligned} \langle \delta z(\mathbf{r}_1, \mathbf{r}_2, t) \delta z^*(\mathbf{r}_1, \mathbf{r}_2, t') \rangle &= \langle \delta z_1(\mathbf{r}_1, t) \delta z_1^*(\mathbf{r}_1, t') \rangle + \langle \delta z_2(\mathbf{r}_2, t) \delta z_2^*(\mathbf{r}_2, t') \rangle \\ &+ \langle \delta z_1(\mathbf{r}_1, t) \delta z_2^*(\mathbf{r}_2, t') \rangle + \langle \delta z_2(\mathbf{r}_2, t) \delta z_1^*(\mathbf{r}_1, t') \rangle. \end{aligned} \tag{101}$$

Since δz_1 and δz_2 are statistically independent,

$$\begin{aligned} &\langle \delta z_1(\mathbf{r}_1, t) \delta z_2^*(\mathbf{r}_2, t') \rangle = \langle \delta z_1(\mathbf{r}_1, t) \rangle \langle \delta z_2^*(\mathbf{r}_2, t') \rangle \text{ and} \\ &\langle \delta z_2(\mathbf{r}_2, t) \delta z_1^*(\mathbf{r}_1, t') \rangle = \langle \delta z_2(\mathbf{r}_2, t) \rangle \langle \delta z_1^*(\mathbf{r}_1, t') \rangle. \end{aligned} \tag{102}$$

In the absence of any offset voltage

$$\langle \delta z_1(\mathbf{r}_1, t) \rangle = \langle \delta z_1^*(\mathbf{r}_1, t) \rangle = \langle \delta z_2(\mathbf{r}_2, t) \rangle = \langle \delta z_2^*(\mathbf{r}_2, t) \rangle = 0, \tag{103}$$

and therefore

$$\langle \delta z(\mathbf{r}_1, \mathbf{r}_2, t) \delta z^*(\mathbf{r}_1, \mathbf{r}_2, t') \rangle = \langle \delta z_1(\mathbf{r}_1, t) \delta z_1^*(\mathbf{r}_1, t') \rangle + \langle \delta z_2(\mathbf{r}_2, t) \delta z_2^*(\mathbf{r}_2, t') \rangle. \tag{104}$$

This means that the autocorrelation function of a signal from the whole scattering volume V is the sum of autocorrelation functions of elementary signals δz from all elementary volumes δV inside V.

Principle of monostatic measurement

In monostatic measurements, altitude profiles of plasma parameters are determined. Then the transmitter cannot work continuously but only during some transmission periods. After transmission, a wave packet travels through the ionosphere causing scattering, which is detected by the receiver.

The propagation of a transmitted pulse can be presented in time-range coordinates as shown in Fig. 17. Modulation means that a continuous sinusoidal signal is multiplied by amodulation envelope (here is a single pulse). The pulse front end travels at a speed c along a line $r = ct$. The rear end starts at a later time and travels along a parallel line. A snapshot of the pulse is a vertical bar. The propagating pulse sweeps all the way through the area between the two tilted lines.

Scattering takes place at all ranges covered by the pulse. Scattering occurring at a single instant of time at different parts of the pulse reaches the transmitter at different times. Hence the signal observed at a single instant of time comes from a fixed point inside the transmitted pulse.

Since the pulse travels upwards, signals from different parts of the pulse scattered at different instants of time will arrive simultaneously at the transmitter site. This is indicated in Fig. 18. It is obvious that the signal at a given instant of time comes from a region with a length of one half of the pulse length.

All this is valid for the signal arriving at the receiver antenna. The receiver acts as a filter calculating weighted averages of the signal. This is demonstrated in Fig. 19, which also shows that the observed signal comes form a region which is longer than one half of the pulse length.

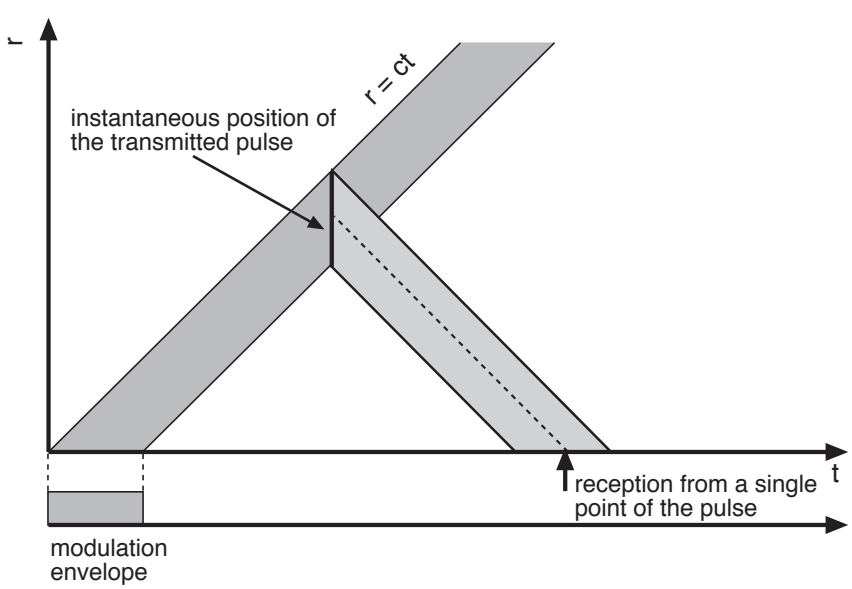

Figure 17: A transmitted radio pulse travelling in the ionosphere and and backscattered signal at the transmitter site.

The modulated transmission signal can be presented as

$$x_t(t) = \epsilon(t) \cdot \cos \omega_0 t, \tag{105}$$

where $\epsilon(t)$ is the modulation envelope. If the scattering signal due to continuous transmission would be $\delta s_i(t)$ from range r_i, the scattering signal due to modulated transmission would obviously be

$$\delta x_i(t) = \epsilon(t - t_0) \cdot \delta s_i(t), \tag{106}$$

where t_0 is the time when the signal from the pulse front reaches the transmitter.

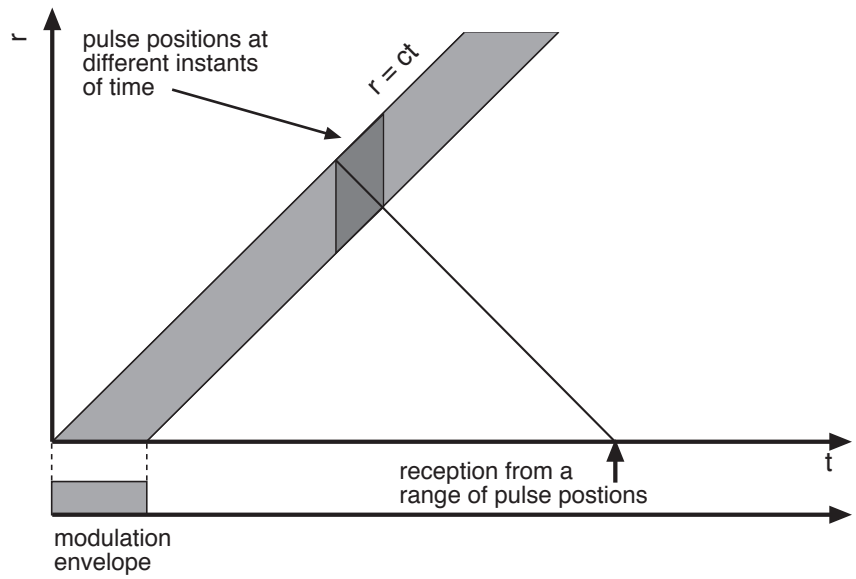

Figure 18: Backscattered signal observed simultaneously from different pulse positions and different instants of time.

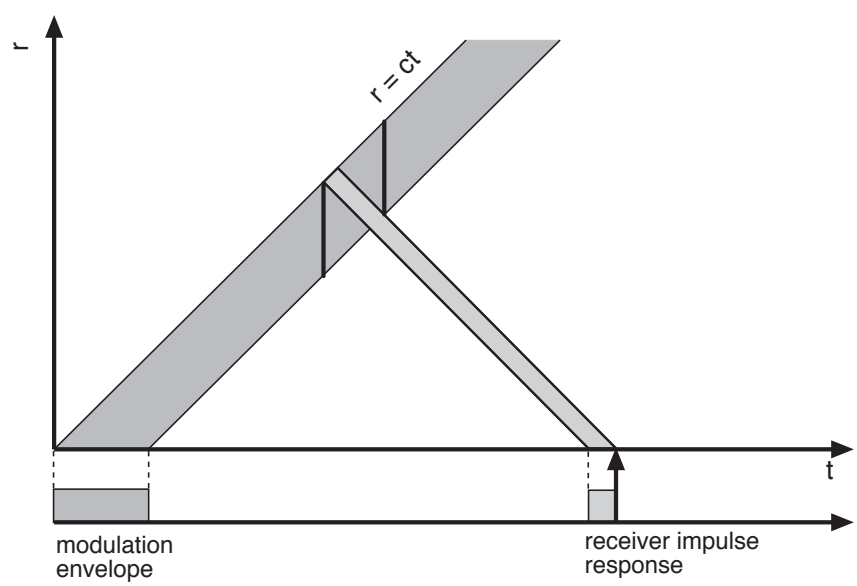

Figure 19: Backscattered signal observed at the rear end of the receiver.

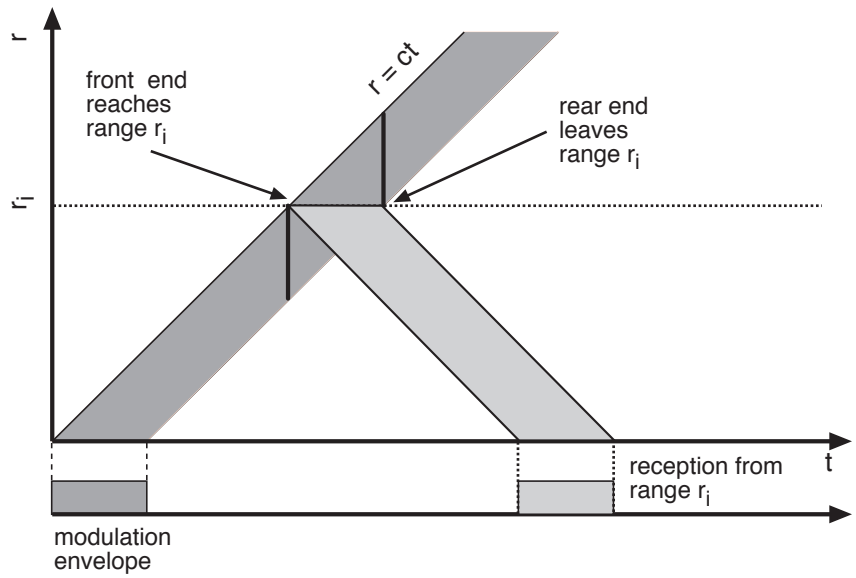

Figure 20: Backscattered signal observed simultaneously from different pulse positions and different instants of time.

Two-dimensional ambiguity function

As seen above, a recorded signal sample contains information on elementary signals from elementary volumes at different ranges. Both radar modulation and receiver filter affect the signal. A problem arises how these two factors affect the signal autocorrelation function, i.e. the signal spectrum. This problem is solved by the theory of ambiguity functions.

When the transmission is modulated with an envelope $\epsilon(t)$, the baseband radar signal (before filtering) from a volume element δV located at a range r is

$$\delta z_\epsilon(t,r) = \epsilon[t - \Theta(r)]\delta z(t,r), \tag{107}$$

where δz is a signal due to continuous monochromatic transmission and

$$\Theta(r) = \frac{2r}{c} \tag{108}$$

is the flight time of the envelope from transmitter to the scattering volume δV and back. The total signal is

$$z_\epsilon(t) = \int \delta z_\epsilon(t,r) = \int \epsilon[t - \Theta(r)]\delta z(t,r). \tag{109}$$

One should notice that both δz and δz_ϵ are stochastic signals. Then the integral in eq. (109) is not an ordinary Riemann integral but a stochastic integral (also known as Itò integral). We can simply take it as a sum of stochastic signals from a large number of small volume elements. Although we formally add signals from all volume elements in the whole space, only those coming from a single macroscopic scattering volume are non-zero.

After downconversion to baseband, the signal passes through the filter at the rear end of the receiver. The filtered signal is

$$\begin{aligned} z_{\epsilon h}(t) &= (z_\epsilon * h)(t) = (h * z_\epsilon)(t) = \int_{-\infty}^{\infty} h(t-\vartheta) z_\epsilon(\vartheta) d\vartheta \\ &= \int_{-\infty}^{\infty} h(t-\vartheta) \left[\int \epsilon(\vartheta - \Theta(r)) \delta z(\vartheta, r) \right] d\vartheta \\ &= \int_{-\infty}^{\infty} \left[\int h(t-\vartheta) \epsilon[\vartheta - \Theta(r)] \delta z(\vartheta, r) \right] d\vartheta, \end{aligned} \tag{110}$$

where h is the impulse response of the receiver. By defining the amplitude ambiguity function

$$W_t^{(A)}(\vartheta, r) = h(t-\vartheta)\epsilon(\vartheta - \Theta(r)), \tag{111}$$

the signal can be written in the form

$$z_{\epsilon h}(t) = \int_{-\infty}^{\infty} \left[\int W_t^{(A)}(\vartheta, r) \delta z(\vartheta, r) \right] d\vartheta. \tag{112}$$

One should notice that a different amplitude ambiguity function is attached to each time of observation. Eq. (112) means that the downconverted and filtered signal is a weighted sum of elementary signals from all volume elements and all times, and the weight in this sum is given by the amplitude ambiguity function. *[Of course, non-zero elementary signals are only obtained from the scattering volume at the crossing of the radar beams, and their amplitudes are controlled by the antenna gains. These effects are contained in $\delta z(\vartheta, r)$. The amplitude ambiguity function introduces an additional spatial weight associated with the length of the radar modulation and also a temporal weight associated with the receiver filtering.]*
According to eq. (112), the signal autocorrelation function is

$$\begin{aligned} \langle z_{\epsilon h}(t) z_{\epsilon h}^*(t') \rangle &= \left\langle \int_{-\infty}^{\infty} \left[\int W_t^A(\vartheta, r) \delta z(\vartheta, r) \right] d\vartheta \cdot \int_{-\infty}^{\infty} \left[\int W_{t'}^{A*}(\vartheta', r) dz^*(\vartheta', r') \right] d\vartheta' \right\rangle \\ &= \int_{-\infty}^{\infty} d\vartheta \int_{-\infty}^{\infty} d\vartheta' \left[\iint W_t^A(\vartheta, r) W_{t'}^{A*}(\vartheta', r') \langle \delta z(\vartheta, r) \delta z^*(\vartheta', r') \rangle \right]. \end{aligned} \tag{113}$$

This contains a double integral of $\langle \delta z(\vartheta, r) \delta z^*(\vartheta', r') \rangle$. Since signals from elementary volumes at different ranges do not correlate, one of the inner integrals disappear and the result is

$$\langle z_{\epsilon h}(t) z_{\epsilon h}^*(t') \rangle = \int_{-\infty}^{\infty} d\vartheta \int_{-\infty}^{\infty} d\vartheta' \left[\int W_t^A(\vartheta, r) W_{t'}^{A*}(\vartheta', r) \langle \delta z(\vartheta, r) \delta z^*(\vartheta', r) \rangle \right]. \tag{114}$$

Using the autocorrelation function of the elementary signal given by eq. (97), this can be put in the form

$$\langle z_{\epsilon h}(t) z_{\epsilon h}^*(t') \rangle = R \int_{-\infty}^{\infty} d\vartheta \int_{-\infty}^{\infty} d\vartheta' \left[\int P_0(r) W_t^{(A)}(\vartheta, r) W_{t'}^{(A)*}(\vartheta', r) \sigma_e(\vartheta - \vartheta', r) d^3 r \right]. \tag{115}$$

Hence, although the radar signal contains a stochastic integral, it disappears when the signal autocorrelation function is calculated. This is understandable, because ensemble average is not a stochastic quantity. The result is that the signal autocorrelation function contains only ordinary Riemann integrals.

By introducing a new variable $\tau = \vartheta - \vartheta'$ we obtain

$$\begin{aligned}\langle z_{\epsilon h}(t) z^*_{\epsilon h}(t')\rangle &= R \int_{-\infty}^{\infty} d\vartheta \int_{-\infty}^{\infty} d\tau \left[\int P_0(r) W_t^{(A)}(\vartheta, r) W_{t'}^{(A)*}(\vartheta - \tau, r) \sigma_e(\tau, \mathbf{r}) d^3 r \right] \\ &= R \int d^3 r P_0 \int_{-\infty}^{\infty} d\tau\, \sigma_e(\tau, r) \left[\int_{-\infty}^{\infty} W_t^{(A)}(\vartheta, r) W_{t'}^{(A)*}(\vartheta - \tau, r)\, d\vartheta \right]. \quad (116)\end{aligned}$$

Here

$$W_{tt'}(\tau, r) = \int_{-\infty}^{\infty} W_t^{(A)}(\vartheta, r) W_{t'}^{(A)*}(\vartheta - \tau, r) d\vartheta \quad (117)$$

i.e. the integral of amplitude ambiguity functions, is called the two-dimensional ambiguity function In terms of this, the signal autocorrelation function is

$$\langle z_{\epsilon h}(t) z^*_{\epsilon h}(t')\rangle = R \int_0^{\infty} P_{0A}(r) \left[\int_{-\infty}^{\infty} W_{tt'}(\tau, r) \sigma_e(\tau, r) d\tau \right] dr, \quad (118)$$

where

$$P_{0A}(r) = \int_{A(r)} P_0(r) dA. \quad (119)$$

The integration in this equation is carried out over $A(r)$, which is the area of the beam cross section at a distance r.

The two-dimensional ambiguity function is a basic concept in the analysis of incoherent scatter data. For each r, it is an unnormalised cross correlation function of the amplitude ambiguity functions for times t and t'. The amplitude ambiguity functions, for their part, depend both on the modulation envelope and the receiver impulse response as indicated by eq. (111). Thus the modulation envelope and receiver impulse response both affect the signal autocorrelation in an inseparable way. The result indicates that each lag $t - t'$ of the signal autocorrelation function has a different two-dimensional ambiguity function.

Instead of r, it is convenient to use $\Theta = 2r/c$ as the second argument of $W_{tt'}$, i.e. $W_{tt'} = W_{tt'}(\tau, \Theta)$.

Example of a single pulse

The modulation envelope of a single pulse is

$$\epsilon(t) = \begin{cases} 1 \text{ , when } 0 < t < T \\ 0 \text{ , when } t \leq 0 \text{ or } t \geq T. \end{cases} \tag{120}$$

We assume a receiver impulse response with a boxcar shape and the same length as the modulation envelope, i.e.

$$h(t) = \frac{\epsilon(t)}{T}. \tag{121}$$

The construction of the amplitude ambiguity function is as follows:

- $W_t^{(A)}(\vartheta, \Theta)$ is defined in ϑ, Θ plane
- $h(t-\vartheta)$ does not depend on Θ and is non-zero within a vertical stripe $t-T < \vartheta < t$
- $\epsilon(\vartheta - \Theta)$ is nonzero within a tilted stripe between the lines $\Theta = \vartheta$ and $\Theta = \vartheta - T$
- the product of these two factors is $W_t^{(A)}(\vartheta, \Theta)$, and it is non-zero where both factors are non-zero; this is an area with a shape of a parallelogram in ϑ, Θ plane.

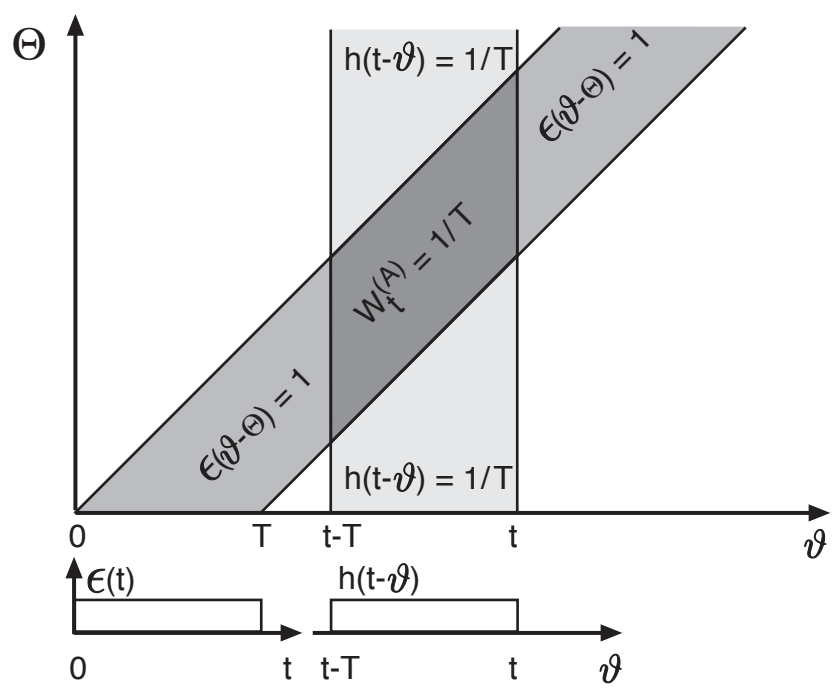

Figure 21: Construction of the amplitude ambiguity function of a single pulse, assuming an impulse response with the same shape.

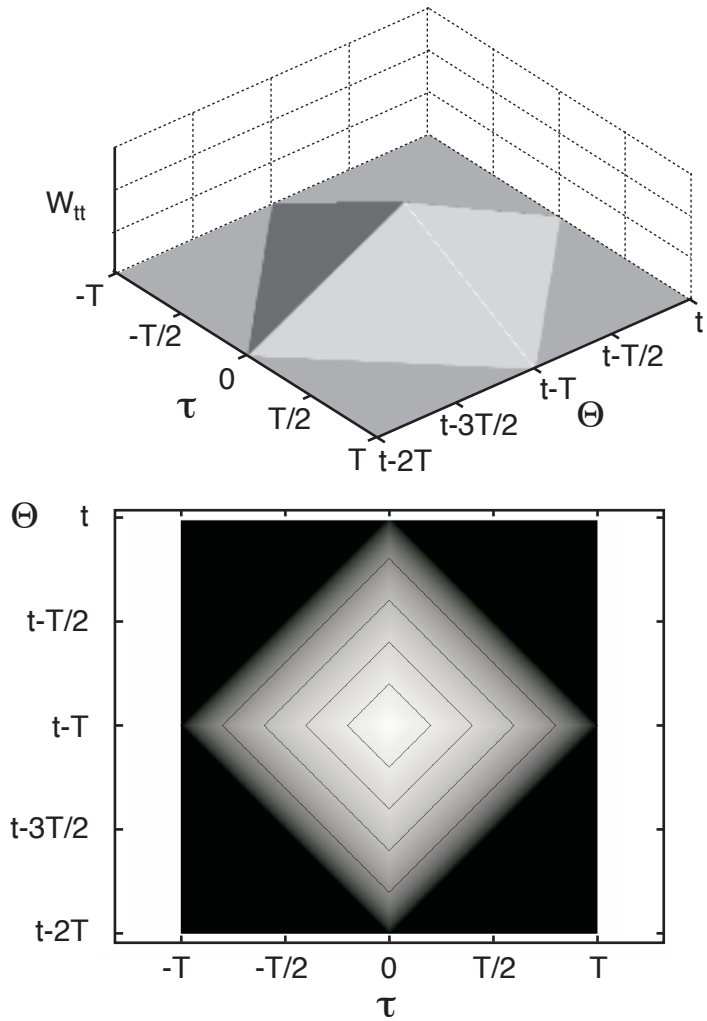

Figure 22: Two-dimensional ambiguity function of zero-lag of a single pulse.

Range ambiguity function

Assume that $W_{tt'}(\tau, \Theta)$ is non-zero within such a narrow range in τ that

$$\sigma_e(\tau, \Theta) \approx \sigma_e(t' - t, \Theta) \tag{122}$$

within that range. Then

$$\begin{aligned}
\langle z_{\epsilon h}(t) z^*_{\epsilon h}(t') \rangle &= R \int_0^\infty P_{0A}(r) \left[\int_{-\infty}^{\infty} W_{tt'}(\tau, r) \sigma_e(t' - t, r) d\tau \right] dr \\
&= R \int_0^\infty P_{0A}(r)\, \sigma_e(t' - t, r) \left[\int_{-\infty}^{\infty} W_{tt'}(\tau, r) d\tau \right] dr \\
&= R \int_0^\infty P_{0A}(r)\, W^{(r)}_{tt'}[\Theta(r)] \sigma_e(t' - t, r) dr, \qquad (123)
\end{aligned}$$

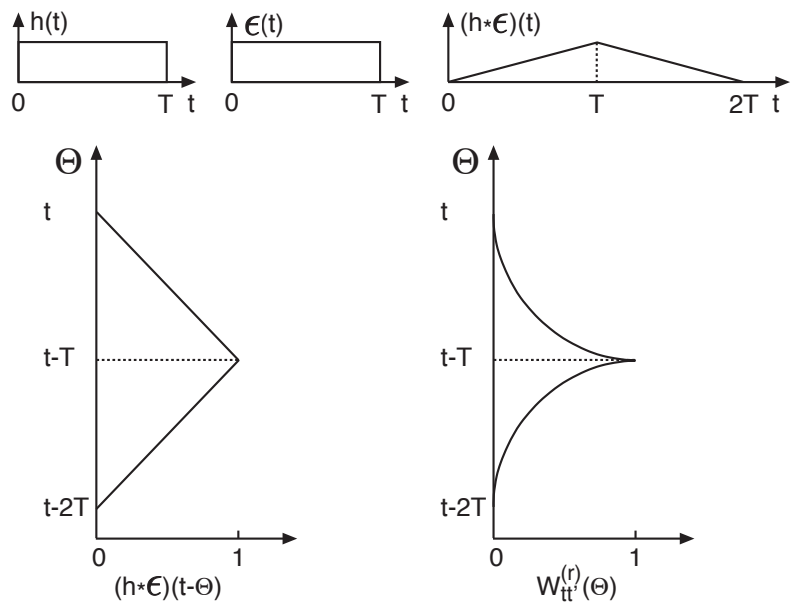

Figure 23: Range ambiguity function of a single pulse.

where

$$W_{tt'}^{(r)}(\Theta) = \int_{-\infty}^{\infty} W_{tt'}(\tau, \Theta) d\tau \tag{124}$$

is the range ambiguity function.

It can be easily shown that

$$W_{tt'}^{(r)}(\Theta) = [(h * \epsilon)(t - \Theta)] \cdot [(h * \epsilon)^*(t' - \Theta)]. \tag{125}$$

This shows that, in order to obtain the range ambiguity function, it is not necessary to calculate the two-dimensional ambiguity function first and then integrate it over the lag variable. Instead, it can be directly calculated from the convolution of the impulse response and the modulation envelope.
Consider a simple pulse and a boxcar impulse response Then $h * \epsilon$ has a triangular shape. Therefore the range ambiguity function for zero lag is a sawtooth peak with sides of parabolic shape.

Spectral ambiguity function

The spectral ambiguity function is defined as

$$\mathcal{W}_{tt'}(\nu,\Theta) = \int_{-\infty}^{\infty} W_{tt'}(\tau,\Theta) e^{2\pi i\nu\tau} d\tau. \tag{126}$$

Because

$$\Sigma_e(\nu,\Theta) = \int_{-\infty}^{\infty} \sigma_e(\tau,\Theta) e^{-2\pi i\nu\tau} d\tau, \tag{127}$$

a direct calculation shows that

$$\int_{-\infty}^{\infty} W_{tt'}(\tau,\Theta)\sigma_e(\tau,\Theta)d\tau \;=\; \int_{-\infty}^{\infty} W_{tt'}(\tau,\Theta)\left[\int_{-\infty}^{\infty} \Sigma_e(\nu,\Theta)e^{2\pi i\nu\tau}d\nu\right]d\tau$$

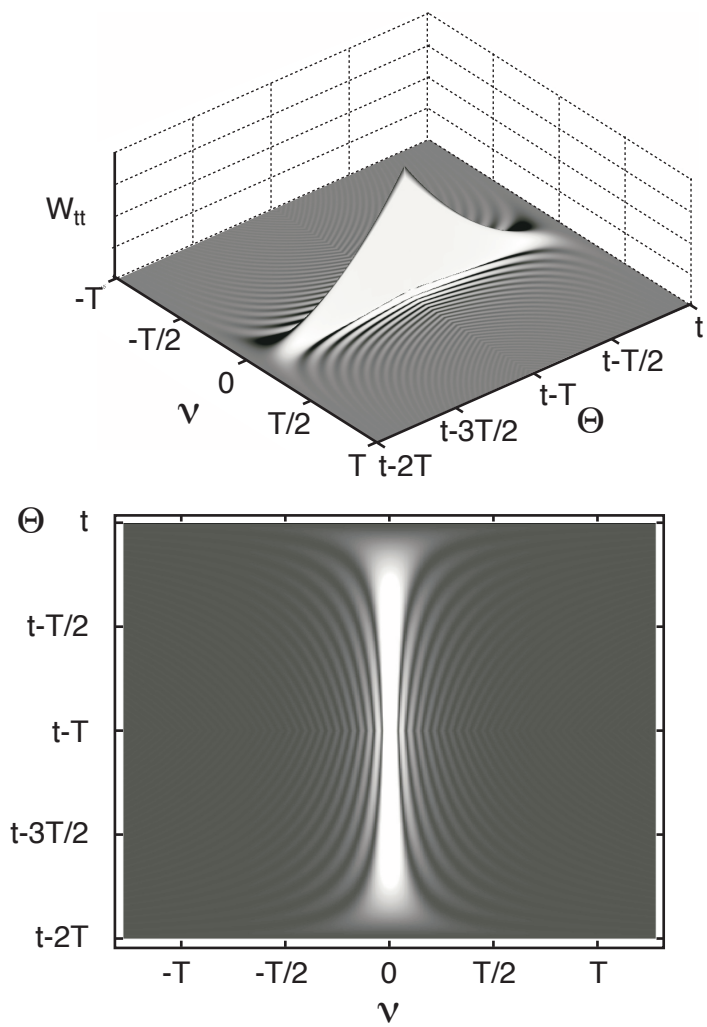

Figure 24: Spectral ambiguity function of zero-lag of a single pulse.

$$
\begin{aligned}
&= \int_{-\infty}^{\infty} \Sigma_e(\nu,\Theta) \left[\int_{-\infty}^{\infty} W_{tt'}(\tau,\Theta) e^{2\pi i \nu \tau} d\tau \right] d\nu \\
&= \int_{-\infty}^{\infty} \Sigma_e(\nu,\Theta) \mathcal{W}_{tt'}(\nu,\Theta) d\nu. \qquad (128)
\end{aligned}
$$

Inserting this in eq. (118) gives

$$
\langle z_{\epsilon h}(t) z^*_{\epsilon h}(t') \rangle = R \int_0^{\infty} P_{0A}(\Theta) \left[\int_{-\infty}^{\infty} \Sigma_e(\nu,\Theta) \mathcal{W}_{tt'}(\nu,\Theta) d\nu \right] d\Theta. \qquad (129)
$$

Determination of plasma parameters

In order to determine the plasma parameters from a given altitude range, one should obtain samples of the radar signal $z_{\epsilon h}(t)$ from this altitude range. Then one should calculate products $z_{\epsilon h}(t) z^*_{\epsilon h}(t')$. When this is repeated a large number of times, the average of these products gives an estimate of $\langle z_{\epsilon h}(t) z^*_{\epsilon h}(t') \rangle$. Then one can use the equation

$$
\langle z_{\epsilon h}(t) z^*_{\epsilon h}(t') \rangle = R \int_0^{\infty} P_{0A}(\Theta) \left[\int_{-\infty}^{\infty} W_{tt'}(\tau,\Theta) \sigma_e(\tau,\Theta) d\tau \right] d\Theta, \qquad (130)
$$

or

$$
\langle z_{\epsilon h}(t) z^*_{\epsilon h}(t') \rangle = R \int_0^{\infty} P_{0A}(\Theta) \left[\int_{-\infty}^{\infty} \Sigma_e(\nu,\Theta) \mathcal{W}_{tt'}(\nu,\Theta) d\nu \right] d\Theta \qquad (131)
$$

or

$$
\langle z_{\epsilon h}(t) z^*_{\epsilon h}(t') \rangle = R \int_0^{\infty} P_{0A}(\Theta)\, W^{(r)}_{tt'}(\Theta) \sigma_e(t'-t, r)\, d\Theta \qquad (132)
$$

for finding the best values of the plasma parameters. This is done by fitting the plasma autocorrelation function $\sigma_e(t'-t, r)$ or scattering spectrum $\Sigma_e(\nu,\Theta)$ to the observed signal autocorrelation function. (Nowadays, methods exist which differ from what is said here.)

The scattering spectrum or plasma autocorrelation function is obtained from the plasma theory. The fitting is non-linear and it must be made using numerical methods (Levenberg-Marquard).

Specific radar modulations and associated filtering are used for obtaining signal from given altitude ranges. The above theory shows that modulaion and filtering are bound together in an unseparable way.

Pulse codes (three-pulse code as an example)

The principle of the three-pulse code is shown in Figs. 25–27. The sampling interval is twice the pulse length and the length of the impulse response is equal to the pulse length. Fig. 25 shows the calculation of $z_i\, z^*_{i+1}$. Each sample contains signal contribution from three different range intervals. The sampling interval is such that two of the range intervals overlap. Samples from these intervals come from the same plasma and therefore they correlate. Signal contributions from the other intervals only produce noise. The measurement gives the signal autocorrelation function at a delay $\tau = 2\mathrm{T}$ (first lag). The ambiguity functions are similar to those for a single pulse.

The principle of obtaining the second lag is shown in Fig. 26. Now every third sample is used in calculating the autocorrelation function estimate. The pulse separations are such that, again, only two range intervals of the two samples overlap. Therefore the autocorrelation function is obtained from this range interval, and the other contributions act as noise. Fig. 27 portrays the generation of the third lag. Now every fourth sample is used in calculating $z_i\, z^*_{i+3}$. Again, correlating signal is obtained only from a single range interval and contributions from other intervals produce self noise. Zero lag of the signal autocorrelation function is obtained using a single pulse.

When the calculation is repeated for different values of i, height profiles of the autocorrelation function at different values of lag are obtained.

In conclusion, the gaps in the three-pulse code have been chosen in such a manner that correlating signals are always obtained from a single range interval when autocorrelation function estimates are calculated for lags $2T$, $4T$ and $6T$. The length of this interval in range is the same as the spatial length of a single pulse. The ambiguity functions for all

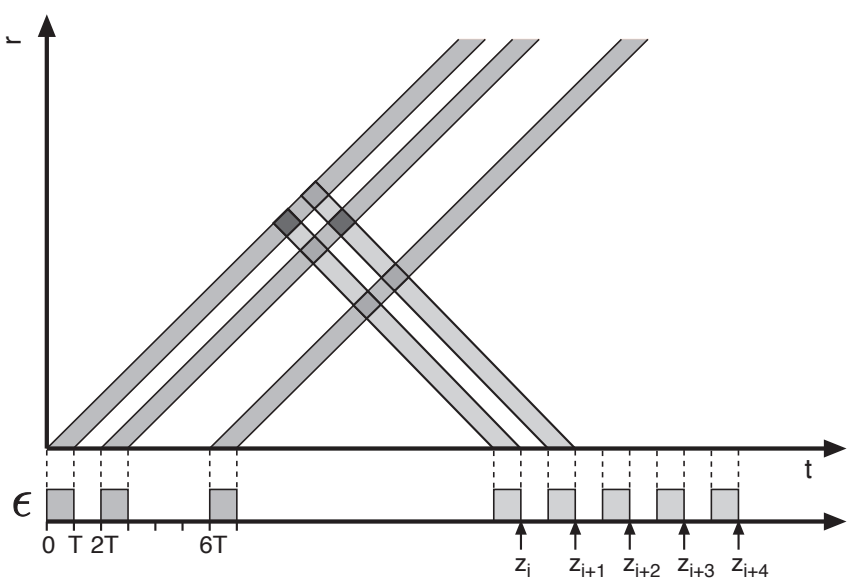

Figure 25: First lag of a three-pulse code.

lags have similar shapes. If the impulse response were a boxcar function, the shapes of the ambiguity functions would be similar to those in Figs. 22 and 23.

The three-pulse code gives only lags 1, 2 and 3. This is not sufficient for practical work, but a larger number of lags is needed in the way demonstrated in Fig. 28. Longer pulse codes exist which are able to give up to ten lags. In the past, five-pulse codes were commonly used, but now they are replaced by more sophisticated modulations. Pulse codes are able to give a range resolution of a few kilometres.

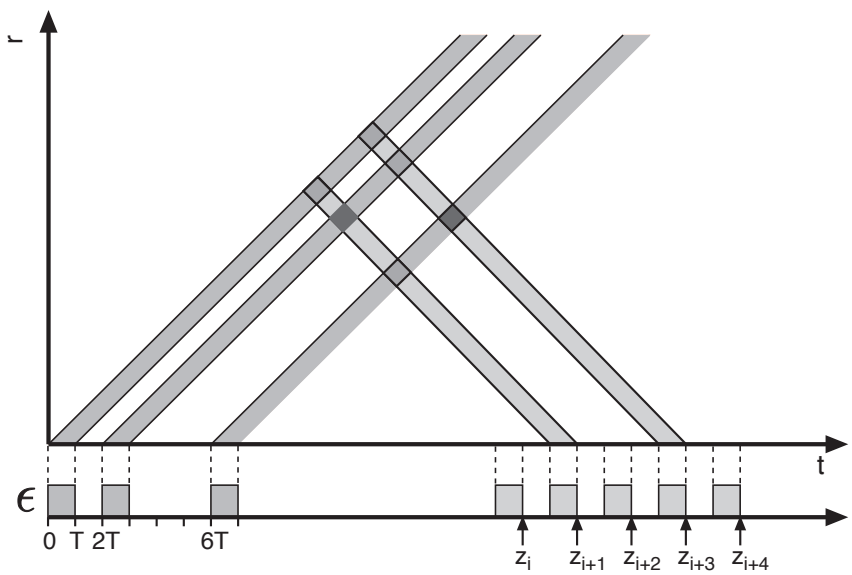

Figure 26: Second lag of a three-pulse code.

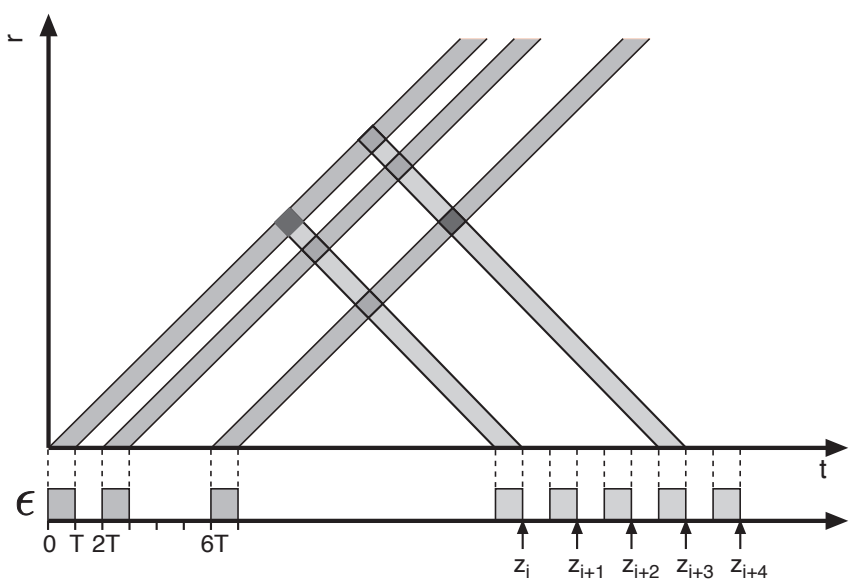

Figure 27: Third lag of a three-pulse code.

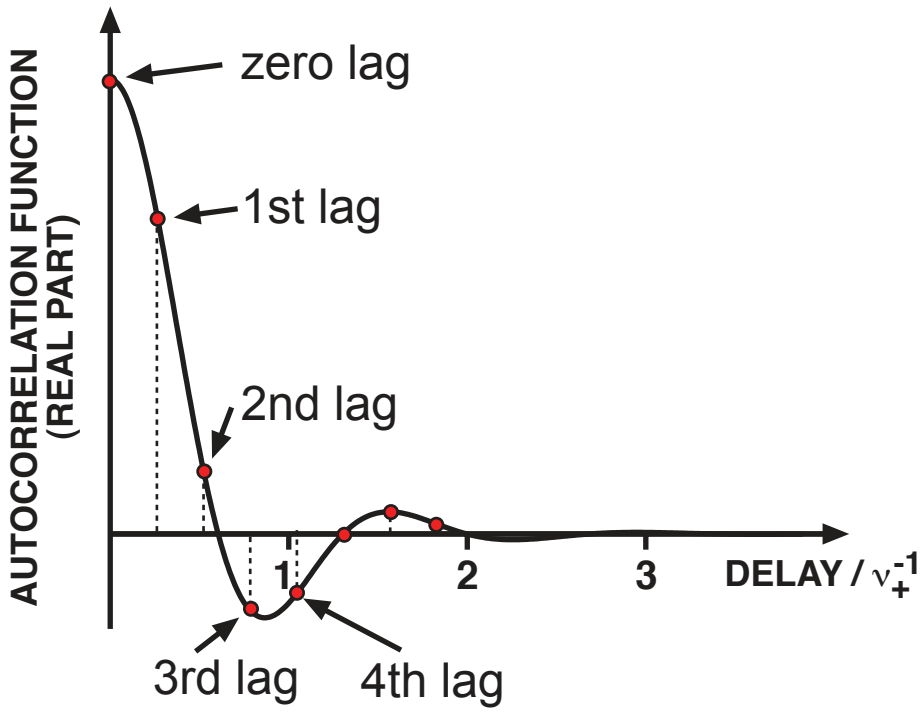

Figure 28: Real part of the signal autocorrelation function at a number of lags.

Barker codes

Improving range resolution beyond the limits put by a reasonable pulse length can be made by means of phase modulation. This means that, e.g. the pulses in a pulse code are divided into shorter elements and the phase of the transmission can be switched by 180° at the boundary between two elements as in Fig. 29.

A phase change of 180° can be obtained by multiplying the original wave from by -1. This can be interpreted as an amplitude modulation envelope of minus unity. Therefore

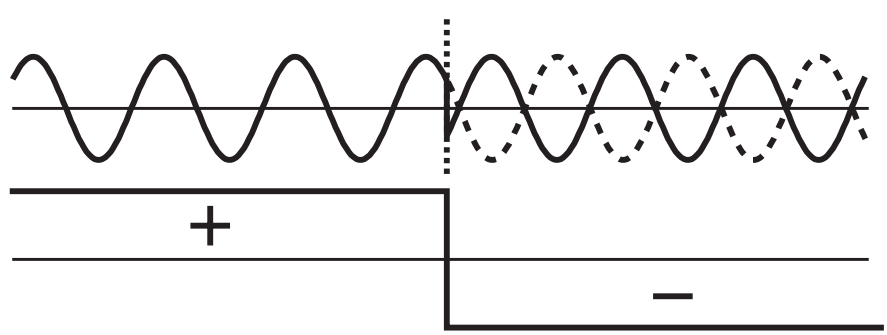

Figure 29: Change of phase by 180°.

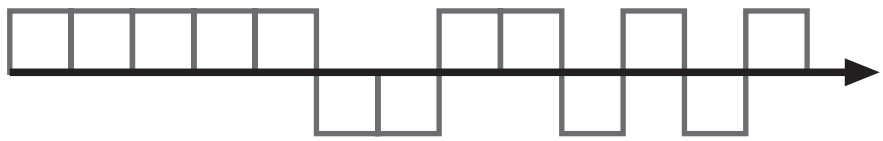

Figure 30: Modulation envelope of a 13-bit Barker code.

a phase code can be written in terms of a sequence of plus and minus signs. 'Plus' means one phase of the transmitter wave form and 'minus' an inverted phase. It is irrelevant which one of the phases is chosen to be 'plus' and which one 'minus'; in this respect the choice is free.

In phase code modulation the phase elements are of equal length. Since one of the two phases is attached to each element, it is reasonable call them bits. A number of different phase codes exist and are also used in incoherent scatter radars. One family of these phase codes are called Barker codes.

Barker codes have a property that their autocorrelation functions have a triangular peak around zero, surrounded by a set of smaller triangular peaks of equal height symmetrically on both sides. A Barker-coded signal is decoded using a matched filter with an impulse response

$$h(t) = \epsilon(-t), \tag{133}$$

where $\epsilon(t)$ is the modulation envelope of the Barker code. Then

$$(h * \epsilon)(\tau) = [\epsilon(-t) * \epsilon(t)](\tau) = \int_{-\infty}^{\infty} \epsilon(\tau + t)\epsilon(t)dt = \mathcal{R}_\epsilon(\tau), \tag{134}$$

where

$$\mathcal{R}_\epsilon(\tau) = \int_{-\infty}^{\infty} \epsilon(\tau + t)\epsilon(t)dt. \tag{135}$$

Thus the range ambiguity function is

$$W_{tt'}^{(r)}(\Theta) = [(h * \epsilon)(t - \Theta)] \cdot [(h * \epsilon)^*(t' - \Theta)] = \mathcal{R}_\epsilon(t - \Theta) \cdot \mathcal{R}_\epsilon(t' - \Theta). \tag{136}$$

For zero lag this reads

$$W_{00'}^{(r)}(\Theta) = \mathcal{R}_\epsilon(-\Theta) \cdot \mathcal{R}_\epsilon(-\Theta) = \mathcal{R}_\epsilon^2(-\Theta). \tag{137}$$

The modulation envelope of a 13-bit Barker code is given in Fig. 30 and the resulting $\mathcal{R}_\epsilon(-\Theta)$ in Fig. 31.
Then, applying eq. (137) gives the range ambiguity function in Fig. 32. This consists of a narrow peak in the middle and tiny sidelobes. The full width of the main peak corresponds to two bit lengths. Without Barker coding the function would be similar to that in Fig. 23, extending from -13 to +13. This means that the effect is nearly the

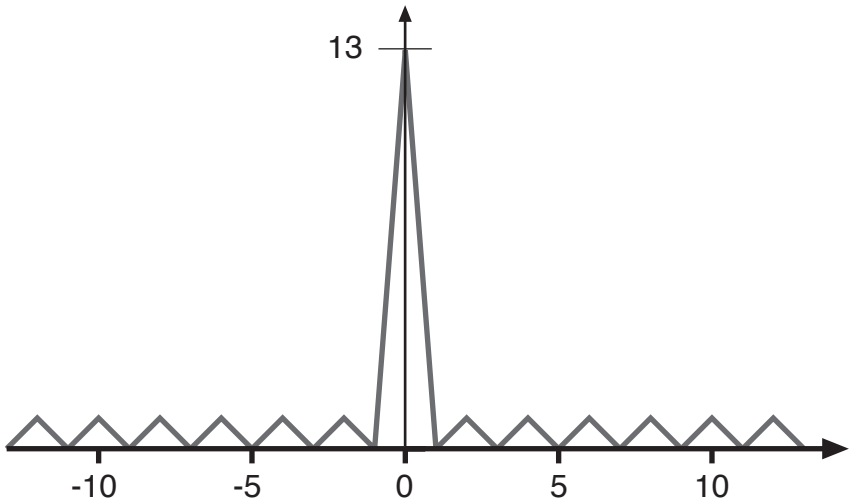

Figure 31: $\mathcal{R}_\epsilon(-\Theta)$ for a 13-bit Barker code.

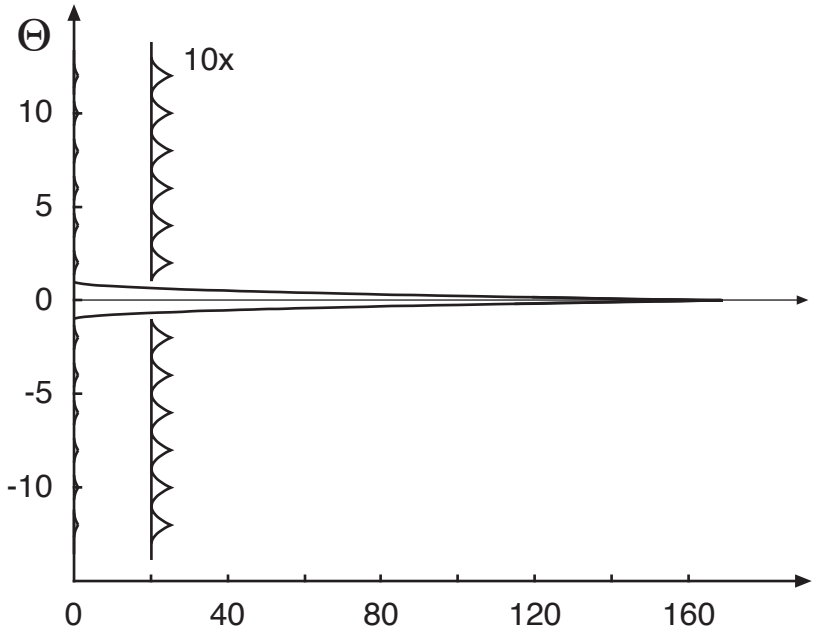

Figure 32: Range ambiguity function of a 13-bit Barker code.

same as compressing the pulse into a single bit and conserving the pulse energy. The two-dimensional ambiguity function is shown in Fig. 33.

A single Barker-coded pulse can be used for measuring the zero lag. The other lags can be obtained with a similar range resolution using Barker-coded pulse codes. An example of such a code is given in Fig. 34. The difference with the unmodulated pulse code is that the gaps between the individual pulses are shorter.

The left hand panel in Fig. 35 shows the convolution of the 13-bit Barker impulse response and the 13-bit three-pulse pattern shown in the right hand panel of Fig. 34. The first lag

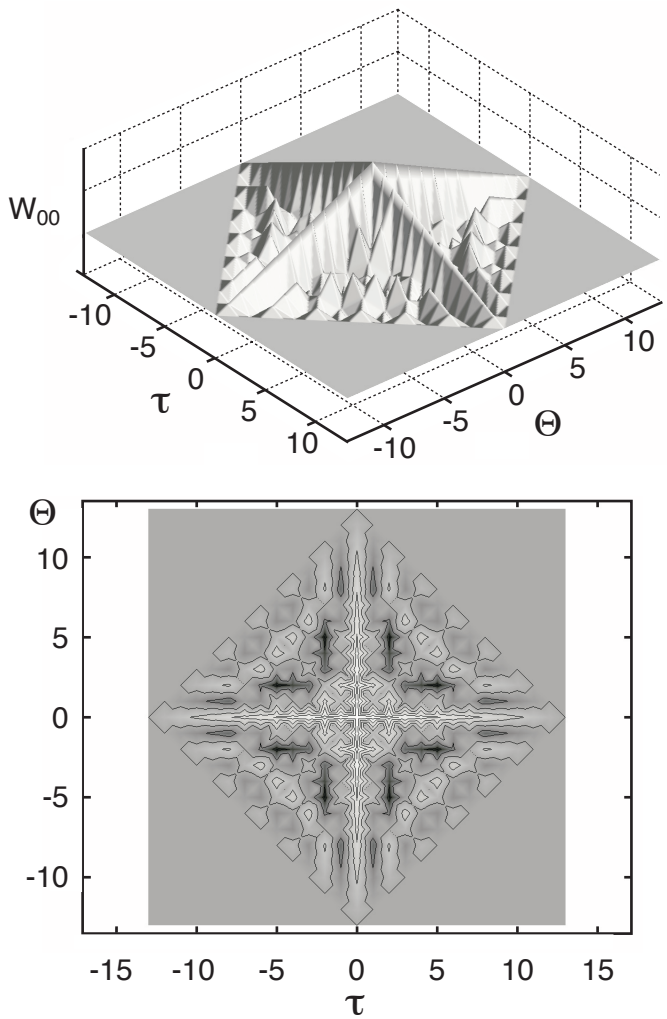

Figure 33: Two-dimensional ambiguity function of a 13-bit Barker code.

is calculated for a single pulse separation which is equal to 13 bit lengths. Hence the first lag is given by

$$W_{t,t+13} = [h * \epsilon(t - \Theta)] \cdot h * \epsilon(t + 13 - \Theta). \tag{138}$$

In Fig. 35 this is gained by shifting a copy of $h * \epsilon(t - \Theta)$ along the Θ axis by 13 bit lengths and multiplying. The range ambiguity function of the third lag is

$$W_{t,t+39} = [h * \epsilon(t - \Theta)] \cdot h * \epsilon(t + 39 - \Theta). \tag{139}$$

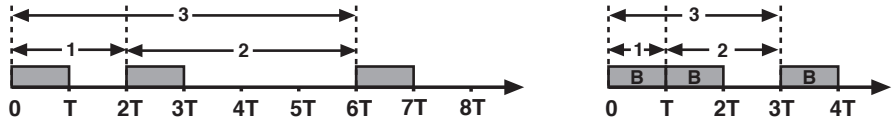

Figure 34: Comparison of plain three-pulse code (left) and a Barker coded three-pulse code (right). Here B indicates any Barker modulation of a pulse.

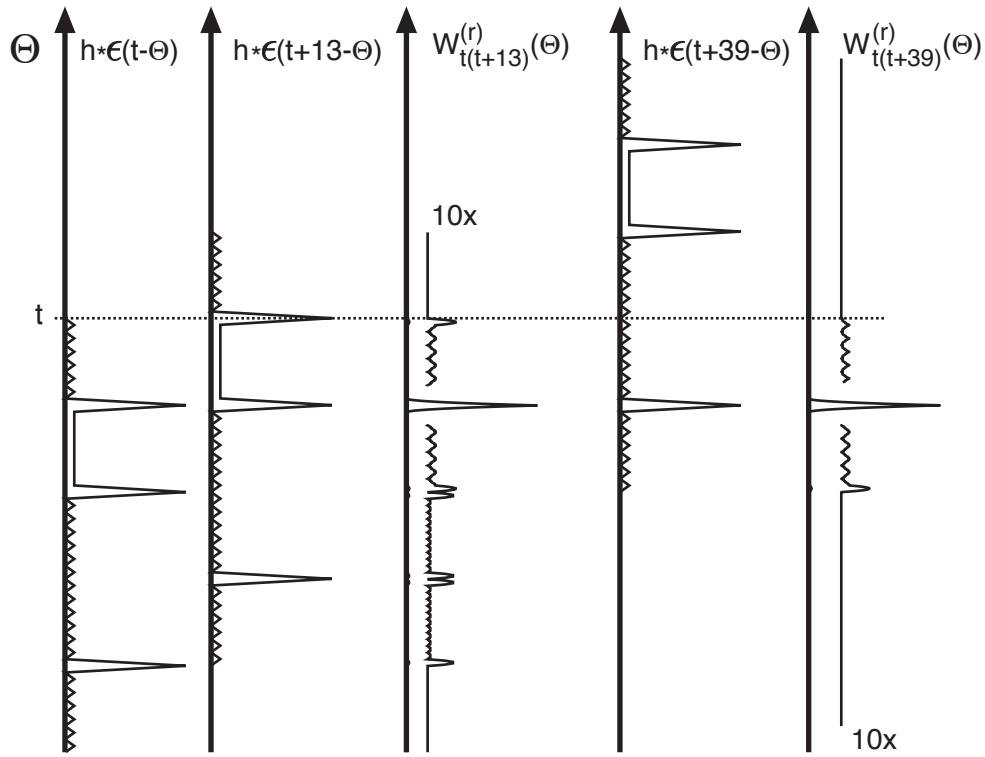

Figure 35: Calculation of the range ambiguity functions of a Barker-coded three-pulse code. A 13-bit Barker code is used.

In this a copy of $h * \epsilon(t - \Theta)$ is shifted by 39 bit lengths. The multiplication gives the range ambiguity function shown in the right hand panel of Fig. 35. This same principle can be used for longer codes.

Alternating codes

Alternating codes are a more modern modulation which gives a high range resolution and is more effective than pulse codes are. The latter results from the fact that alternating codes contain no gaps and therefore they utilize the radar duty cycle more effectively than pulse codes do.

Alternating codes are phase codes which use two phase values, 0° and 180°. They consist of a cycle of long pulses, which are divided into a number of bits. Reception takes place after each transmission before the next pulse is transmitted. The phase patterns change from pulse to pulse and the length of the impulse response is equal to the bit length rather than pulse length. When all pulses are transmitted, the sequence is repeated all over again.

The codes work in power domain rather than in amplitude domain. This means that the process corresponding to decoding is not done in terms of amplitudes (like in Barker coding) but in terms of lagged products; lagged products from successive pulses are added and

subtracted according to certain rules so that the corresponding ambiguity functions cancel except at a single short altitude range corresponding to the bit length. The modulations of alternating codes make a finite set which is repeated all over again.

Alternating codes are divided into two types, weak and strong. Weak codes are applicable if each bit of the code is further modulated by a Barker code, otherwise strong codes must be used. The number of bits in both codes is equal to a power of two. The cycle length of a weak code is equal to the number of bits in a single phase pattern and that of a strong code twice the number of bits. In practice, only strong codes are nowadays used even when Barker submodulation is applied.

The working principle of alternating codes can be demonstrated in terms of a four-bit weak code as shown in Fig. 36. The modulation envelopes of the four transmissions of the cycle are shown by pluses and minuses on the four rows in the left hand panel. The four rows together make the whole cycle. The rows, i.e. the phase patterns of the individual pulses, are sometimes called scans and their order in the cycle is indicated by a number called the scan count.

The matrix in the second panel ($W_1^{(r)}$) is obtained by multiplying the successive columns in the original sign matrix in the left hand panel; the first column is the product of the first and second, the second a product of second and third, and the third a product of third and fourth.

The next panel is obtained from $W_1^{(r)}$ by multiplying all its columns by the first column so that the first column will be all pluses. When the sums of the three columns are calculated, it turns out that only the first column will give a non-zero result (equal to 4), while the pluses and minuses cancel in the other two columns. The last two panels are obtained in a similar manner using the signs of the second and third column of $W_1^{(r)}$. Also in these two cases the sums of only a single column (second and third) are non-zero.

For interpreting this result, assume that the signal is sampled at intervals equal to the bit length. After each transmission, a different set of samples and lag estimates is obtained.

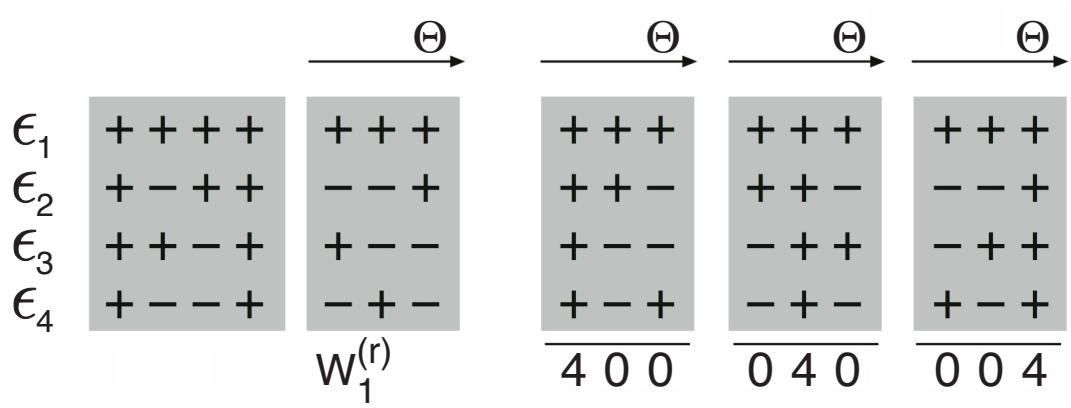

Figure 36: The working principle of a weak alternating code.

If the impulse response of the system is equal to the Dirac δ, each row in the matrix $W_1^{(r)}$ simply corresponds to multiplication of two $h * \epsilon$ terms separated by a single bit length on the Θ axis. Therefore the pluses and minuses on each row indicate the values of the range ambiguity functions of lag estimates $z_i z_{i+1}^*$ at integer values of Θ.

If lag estimates $z_i z_{i+1}^*$ are calculated for each scan of and they are added and subtracted in using the the same signs as those in calculating the three last panels in Fig. 36, the range ambiguity functions will add and cancel as shown in the figure. Hence the results will contain information from the range extent of a single bit length only. There are three different ways of making this calculation and each of them will give a result from a different range interval. Thus adding and subtracting range ambiguity functions will lead to ambiguity functions similar to those of a simple two-pulse code. Since this can be done in three different ways, two successive data samples give first lag estimates at three different ranges. These correspond to the three bit pairs which have a separation of a single bit length in a four-bit sequence.

The second and third lag can be studied in a similar way by calculating the matrices $W_2^{(r)}$ and $W_3^{(r)}$, which consist of two columns and a single column, respectively. Because a four-bit sequence contains two bit pairs with a separation of two bit lengths, $z_i z_{i+2}^*$ will give second lag estimates at two ranges. Similarly, $z_i z_{i+3}^*$ gives only a single third-lag estimate, since only the separation of the first and fourth bit is equal to three bit lengths. When lags 1–3 are calculated for all data samples z_i in this manner, three lag estimates will be obtained at each range gate for the first lag, two for the second lag and one for the third lag.

Longer weak codes work in an analogous way. The code length is a power of two. For an n-bit code, $n - i$ lag estimates will be obtained for the ith lag. The zero lag cannot be determined with the same height resolution, but it contains range ambiguities much in the same way as the zero lag of a multipulse code does.

Here the impulse response was Dirac δ, so that the neighbouring bits are separate in calculating $h * \epsilon$. With a realistic impulse response the successive bits would be mixed and the conclusions are no more valid. However, applying Barker coding to individual bits makes the range ambiguity functions consist of narrow peaks and weak sidelobes. The principle is similar to the use of Barker codes in multipulses. Since $h * \epsilon$ consists of a single high peak with small sidelobes, the different range ambiguity functions will also consist of a set of peaks, and adding and subtracting them will lead to effective range ambiguity functions with a single main peak only.

Barker submodulation is not needed in strong alternating codes. The number of scans in strong codes is twice the number of bits so that a four-bit strong code corresponding to the weak one in Fig. 36 contains eight scans.

Modulation envelopes of a four-bit strong code are shown in the left hand panel of Fig. 37 and their convolutions with a boxcar-shaped impulse response in the right hand panel. The length of the impulse response is equal to the bit length.

When the sampling interval is equal to the bit length, the range ambiguity functions of the first lag of the eight modulation envelopes in Fig. 37 are as shown in Fig. 38. These

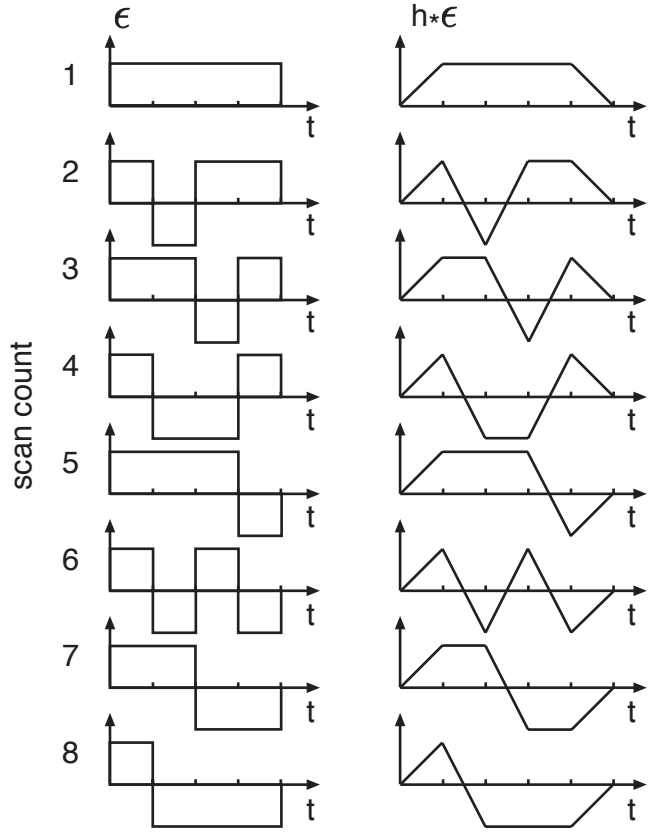

Figure 37: Strong four-bit alternating code sequence and convolutions with a boxcar impulse response.

can now be added and subtracted in the same way as in Fig. 36. If a sign sequence $+-+-+-++$ is used for the eight scans, the ambiguity functions cancel except within an interval of the peak shown in the first panel of the decoded range ambiguity functions on the right hand side of the figure. The shape of this ambiguity functions is the same as that of a single pulse pair. Using sign sequences $+--++--+$ and $++----++$ lead to similar range ambiguity functions, but at a different ranges. Hence the same data samples are able to give the first lag at three different ranges and the range resolution is determined by the length of a single bit in the modulation envelope.

The range ambiguity functions of the second lag are shown in Fig. 39. They are now shorter than the first-lag ambiguity functions. The decoding is now made by means of sign sequences $+----++--$ and $+-----+-+$, which leads to two range ambiguity functions at two different ranges.

Finally, the range ambiguity functions of the third lag are plotted in Fig. 40. Ih this case decoding produces a range ambiguity function at a single range only, but the shape if this function is similar to that of a two-bit code.

A pulse divided into four bits contains three subsequent bit pairs, two bit pairs with

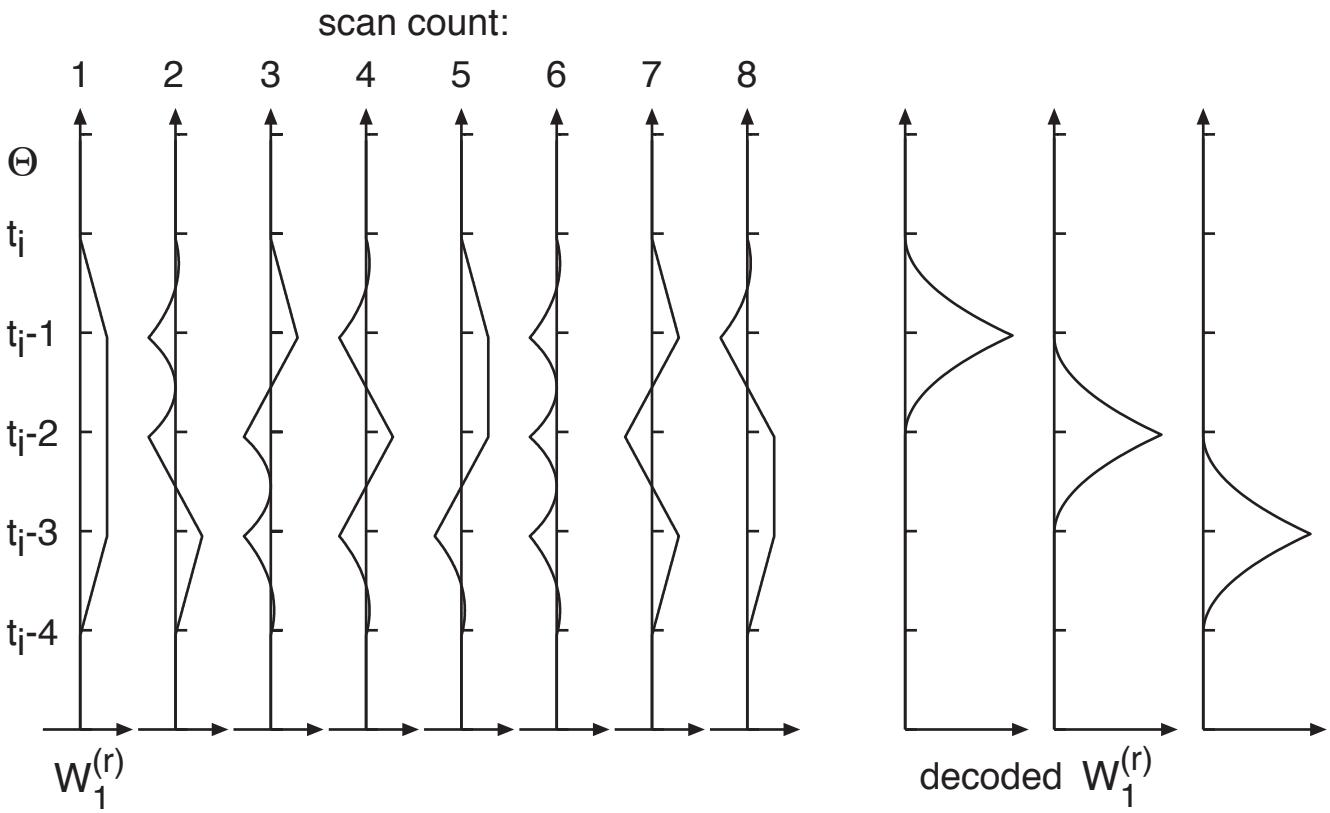

Figure 38: Left panel: Range ambiguity functions of the first lag for the modulation envelopes of the four-bit alternating code sequence in Fig. 37. Right panel: Corresponding decoded range ambiguity functions.

one bit in between and a single bit pair with two bits in between. The calculated range ambiguity functions indicate that the alternating code sequence is able to produce range ambiguity functions corresponding to each one of these bit pairs. One should also notice that similar results would not be obtained by transmitting separately two-pulse codes corresponding to these bit pairs. For instance the bits giving the first lag have no gap in between. Due to the effect of the filter impulse response, this would lead to a range ambiguity. Hence the strong alternating code is clever enough to avoid the gaps which are needed in pulse codes.

The decoded two-dimensional ambiguity functions of all lags of the four-bit strong alternating code are shown in Fig. 39. The functions for all lags 1, 2 and 3 consist of pyramids like those given by multipulse codes. Unlike in multipulse codes, however, they partly overlap and the topmost surface is only visible in the figure. The zero lag ambiguity function is also shown, and it is a ridge elongated in Θ direction.

The strong four-bit code has not much practical value. This is because it gives only three lags. Longer codes are available which give sufficient lag and range resolutions.

The alternating code principle can only work for specific sign sequences. Finding these

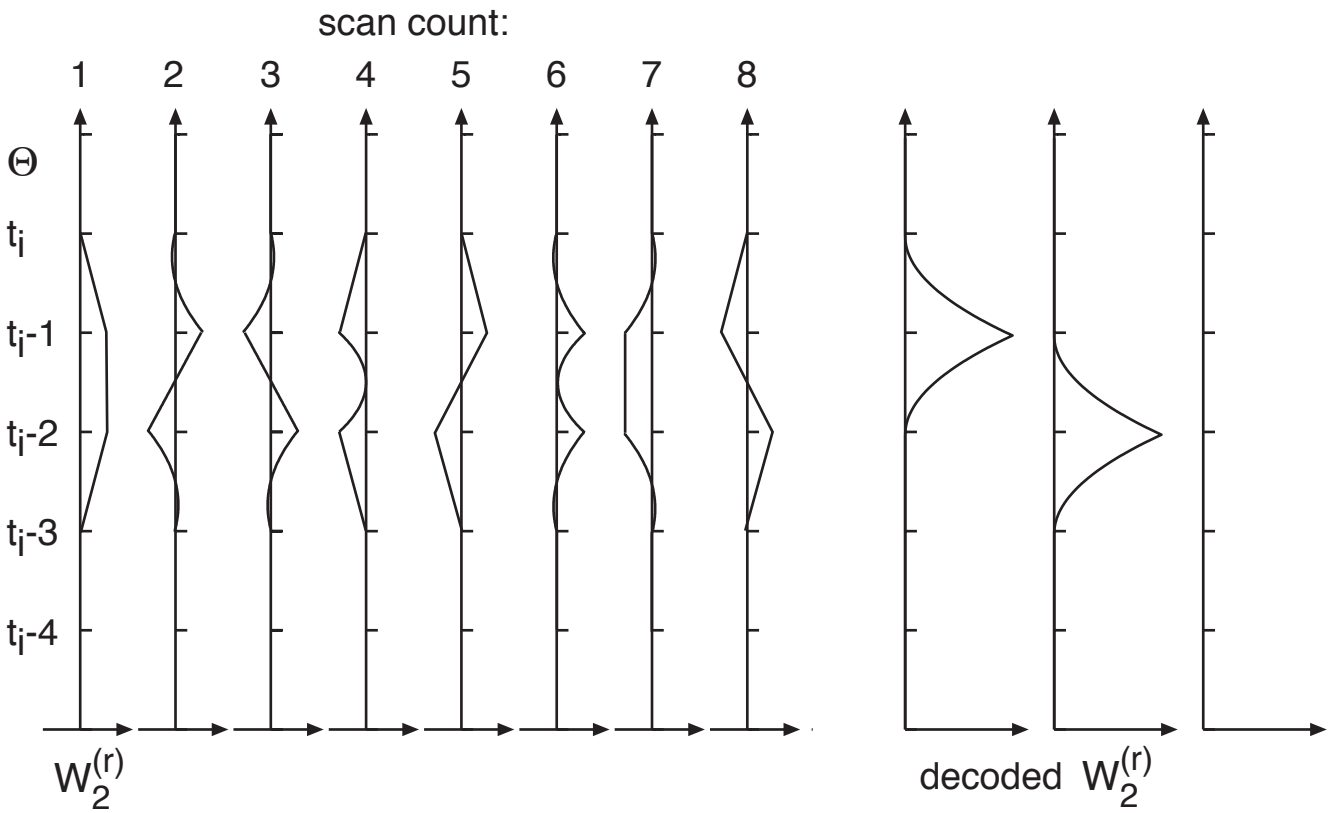

Figure 39: Same as Fig. 38 for the second lag.

sequences is a major problem. Consider, for example, a strong four-bit code. The number of possible combinations is $2^{4\times 8} = 2^{32} \approx 4.3 \cdot 10^9$. If your computer is able to test one combination in 0.01 s, testing all possibilities would take 1.4 years. In the case of an eight-bit code the number of combinations is $2^{8\times 16} = 2^{128} \approx 3.4 \cdot 10^{38}$ and the time needed would be about 10^{30} years. This is a long time in comparison with the age of the universe (about $14 \cdot 10^9$ years). In spite of these pessimistic views, very long alternating codes have been found, up to a length of 4194304 bits. This, of course, is much more than needed in any practical application.

The code search is based on Walsh matrices. The starting point for an n-bit strong alternating code is a $2n \times n$ Walsh matrix. The idea is that, by picking correctly a set of columns form a Walsh matrix in a proper order and putting them into columns of a new matrix, the resulting matrix contains the signs of an alternating code sequence, each modulation envelope on a single row. In searching an n-bit strong code, one half of the columns of a $2n \times 2n$ Walsh matrix are used. The columns of the Walsh matrix are numbered starting from zero. It is practical to use octal numbering. These numbers are called Walsh indices. Thus an alternating code can be written down as a sequence of Walsh indices. An example of this idea is shown in Fig. 42 for an 8-bit strong alternating code.

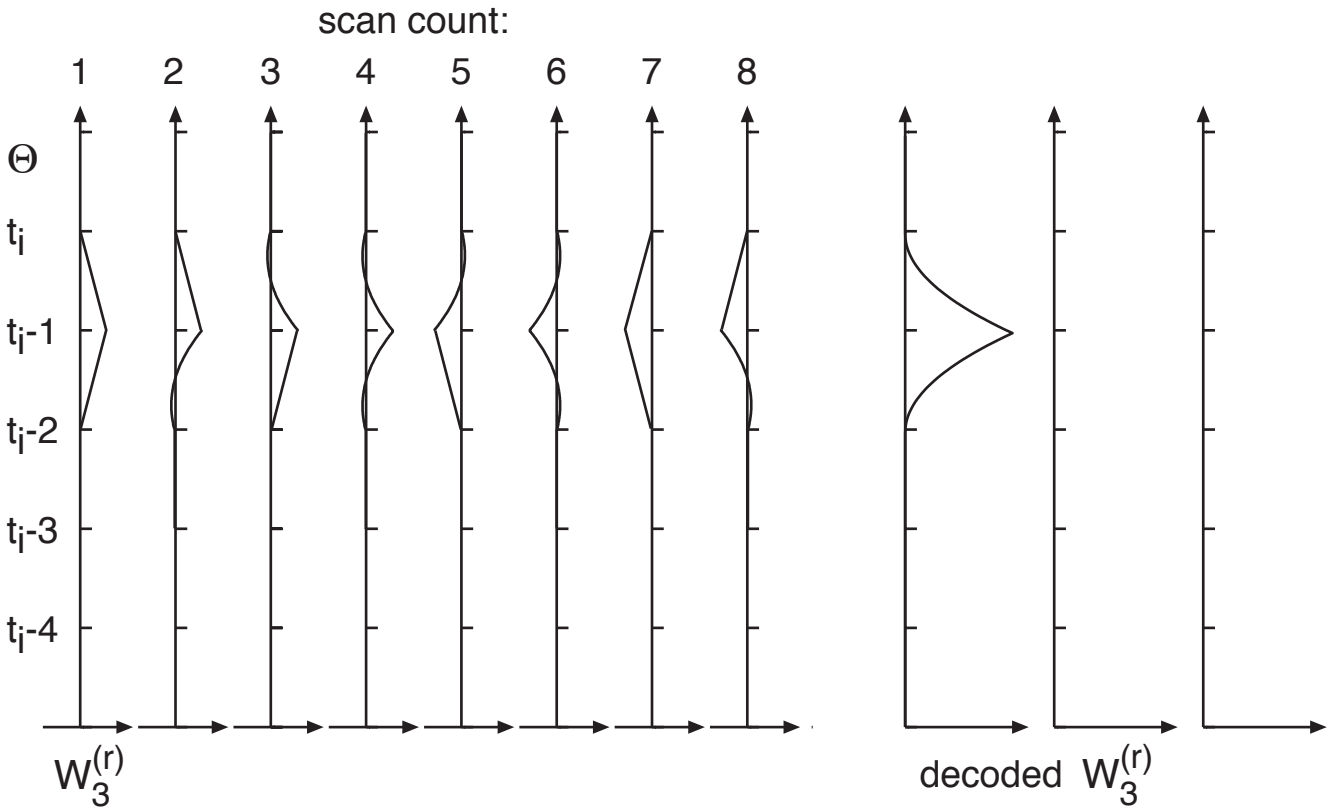

Figure 40: Same as Fig. 38 for the second lag.

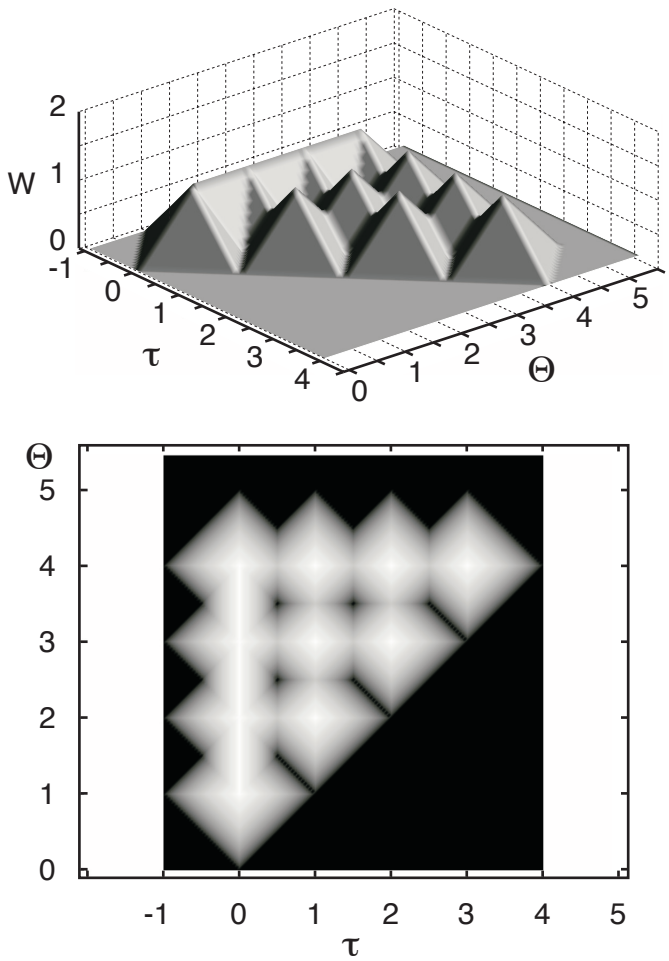

Figure 41: Two-dimensional ambiguity functions of a four-bit strong alternating code code.

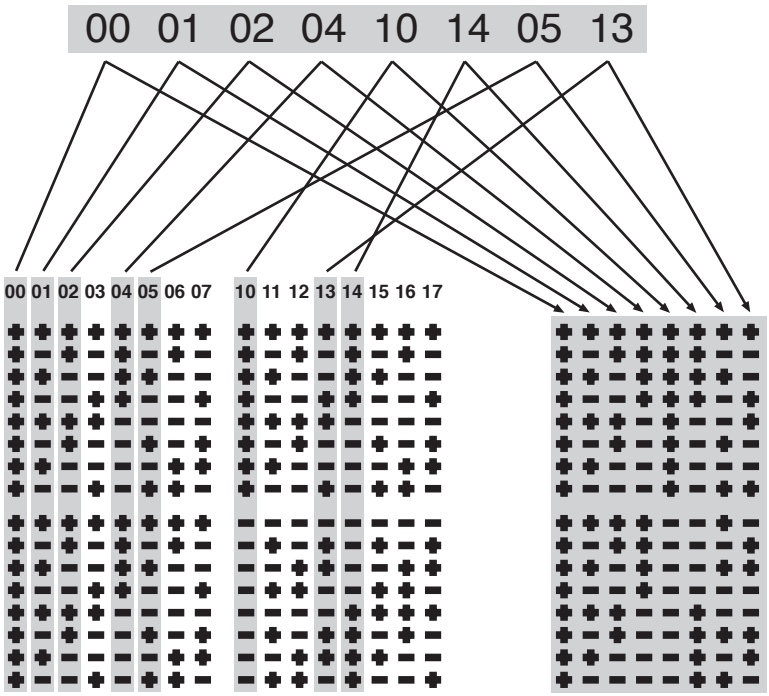

Figure 42: Constructing an 8-bit strong alternating code from a Walsh sequence.